Electrocatalysts Based on Metal@Carbon Core@Shell Nanocomposites: an Overview

Yi Peng and Shaowei Chen*

Department of Chemistry and Biochemistry, University of California, 1156 High Street, Santa Cruz, California 95064, USA. * E-mail: shaowei@ucsc.edu

Abstract

Developing low-cost, high-performance catalysts is of fundamental significance for electrochemical energy conversion and storage. In recent years, metal@carbon core@shell nanocomposites have emerged as a unique class of functional nanomaterials that show apparent electrocatalytic activity towards a range of reactions, such as hydrogen evolution reaction, oxygen evolution reaction, oxygen reduction reaction, and CO_2 reduction reaction, that are important in water splitting, fuel cells and metal-air batteries. The activity is primarily attributed to interfacial charge transfer from the metal core to the carbon shell that manipulate the electronic interactions between the catalyst surface and reaction intermediates, and varies with the structures and morphologies of the metal core (elemental composition, core size, etc.) and carbon shell (doping, layer thickness, etc.). Further manipulation can be achieved by the incorporation of a third structural component. A perspective is also included highlighting the current gap between theoretical modeling and experimental results, and technical challenges for future research.

Keywords: metal@carbon core@shell nanocomposite; electrocatalysis; hydrogen evolution reaction; oxygen evolution reaction; oxygen reduction reaction

1. Introduction

In recent decades, extensive research efforts have been devoted to the development of effective technologies for electrochemical energy conversion and storage, which entail, in particular, rational design and engineering of functional nanomaterials as high-performance, low-cost catalysts towards important reactions, such as hydrogen evolution reaction (HER), oxygen evolution reaction (OER), oxygen reduction reaction (ORR), and carbon dioxide reduction reaction (CO_2RR) [1-7]. Currently, the leading catalysts for these reactions are generally based on noble metals such as platinum, ruthenium and iridium [8-12], where structural engineering represents a key strategy to enhance the performance and concurrently reduce the costs of the catalysts [13-18]. This has been demonstrated in a number of prior studies that focus on the manipulation of the elemental compositions, crystalline facets, surface morphologies, as well as alloying of the nanoparticles with (non-)noble metals [19-26]. In some other studies [2, 27-31], nanocomposites based on (non-noble) metals and metal compounds incorporated into carbon matrices have also been found to exhibit apparent electrocatalytic activity. For instance, Wang and coworkers [2] summarized non-noble metal-based carbon composites as HER electrocatalysts and the activity was attributed to (i) improved electrical conductivity by the carbon phase and texture structures, (ii) the formation of abundant active sites due to high dispersion of small-sized metal/metal composites on carbon, and (iii) charge transfer dynamics facilitated by the synergistic coupling between the two components. The Chen group [31] reviewed single metal atoms supported on a carbon matrix as efficient electrocatalysts, and Asefa et al. [27] summarized (noble) metal-free heteroatom-doped carbons as high-performance electrocatalysts. Among these, metal@carbon (M@C) core@shell composites, where metal nanoparticles are encapsulated within a carbon matrix, have been attracting particular interest because of their unique features, such as high electrical conductivity, large surface area, and optimizable surface electronic structure due to intimate interactions between the metal core and carbon shell [32-35]. The encapsulation of the metal nanoparticles within a carbon shell also leads to enhanced structural stability of the metal and thus long-term durability of the catalysts [36-46]. In this review, we will focus on recent progress in the design and engineering of M@C electrocatalysts towards diverse reactions (Fig. 1), within the context of the metal cores, carbon shells, and third components.

We will start with an overview of theoretical advances that help develop a mechanistic framework

of M@C composites in electrocatalysis, summarize recent progress in the design and engineering of various M@C structures for diverse applications, and then include a perspective that highlights key challenges in future research.

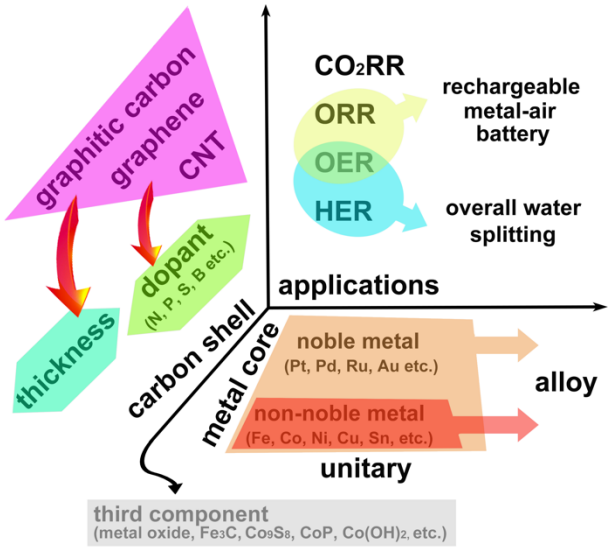

Figure 1. An overview illustration of the M@C composites, where the metal core can be a noble metal (Pt, Pd, Ru, Au, etc), non-noble metal (Fe, Co, Ni, Cu, Sn, etc.), or their alloy, and the carbon shell varies in thickness, ranging from carbon nanotube (CNT), to graphene, and graphitic carbon with or without dopants (N, P, S, B, etc). These catalysts can be used for ORR, OER, HER and CO_2RR, and devices like overall water splitting and rechargeable metal-air battery. A third component material like metal oxide, Fe_3C, Co_9S_8, CoP, $Co(OH)_2$, etc, can also be integrated as part of the core or shell, or with the M@C materials forming a more complicated composite structure with a further enhanced performance.

2. Mechanistic framework

To rationally design high-performance, advanced electrocatalysts, it is of fundamental importance to understand the reaction pathways and identify catalytic active sites, in which density functional theory (DFT) calculations have been playing a powerful role [47-52]. For instance, M@C nanocomposites have been known to be active towards HER, which in general entails three key reactions in acid,

$$\text{Volmer reaction: } * + H^+ + e^- \leftrightarrow H^* \quad (1)$$
$$\text{Tafel reaction: } 2H^* \leftrightarrow H_2* \quad (2)$$
$$\text{Heyrovsky reaction: } * + H^+ + e^- + H^* \leftrightarrow H_2* \quad (3)$$

where * is the active site of the catalyst. Results from DFT calculations have shown that the HER process likely involves the Volmer-Heyrovsky or Volmer-Tafel pathway on a range of transition-metal surfaces, where the Volmer step is a fast reaction while the Heyrovsky or Tafel reaction is the rate-determining step [53-55]. In 1958, Parson first pointed out that a maximum exchange current density would be attained when the hydrogen adsorption free energy (ΔG_{H^*}) was close to thermoneutral ($\Delta G_{H^*} \sim 0$) [56]. Norskov et al. plotted ΔG_{H^*} from DFT calculations versus experimental HER exchange current density (Fig. 2) [57], and observed a volcano-shaped variation with the peak position close to platinum — note that platinum is the state-of-the-art HER catalyst with an almost zero overpotential and small Tafel slope. This volcano plot was further consummated in other studies in the literatures [58, 59]. This suggests that ΔG_{H^*} can be exploited as an effective descriptor in the design, engineering and optimization of HER catalysts. For M@C catalysts, with the active sites located on the carbon shell, one can see that whereas ΔG_{H^*} on pure C is very positive and H^+ adsorption (Volmer step) is energetically unfavorable, in contrast to transition metals where ΔG_{H^*} is generally negative, the formation of M@C core@shell structures leads to reduced ΔG_{H^*} on the C shell, in good agreement with enhanced HER activity observed experimentally. This is

largely attributed to effective charge transfer from the metal core to the carbon shell [60]. Further contributions can arise from deliberate doping of the carbon shells by select metal and nonmetal heteroatoms. Fig. 3 depicts results from DFT calculations of N-doped graphitic carbon hybridized with various transition metals (compounds) in HER electrocatalysis [61]. The atomic structures of the hybrids of N-doped graphene (NG) supported on substrates like Co (111), Fe (110), Co_3O_4 (111), Fe_3O_4 (111), WC (0001) and VC (111) are illustrated in Fig. 3a, with the corresponding ΔG_{H^*} shown in Fig. 3b. One can see that ΔG_{H^*} of undoped graphene (G) is very positive at +1.84 eV, suggesting difficult adsorption of proton. Introduction of N dopants into G (NG) markedly lowers the ΔG_{H^*} to +0.54 eV. For comparison, ΔG_{H^*} is −0.48 eV on Co (111); and in the NG/Co hybrid, ΔG_{H^*} is reduced to +0.13 eV on the C sites adjacent to N dopant and on the hollow site of Co substrate, a condition favored for HER. Fig. 3c further compares the ΔG_{H^*} of NG on other substrates, where the proton binding strength can be seen to follow the order of NG/Fe > NG/VC ~ NG/WC > NG/Co > NG/Co_3O_4 > NG/Fe_3O_4 ~ NG/TiC. This is accounted for by electron injection from the substrates to the graphitic sheet that breaks the π conjugation by occupying the carbon p_z orbitals. This can be described by the center of the C p_z band by the following equation, $\varepsilon p_z = \frac{\int_{-\infty}^{0} ED(E)dE}{\int_{-\infty}^{0} D(E)dE}$, where D(E) is the DOS of the C p_z band at a given energy. Interestingly, the εp_z values of the hybrids shows a linear relationship with the corresponding ΔG_{H^*} (Fig. 3d), suggesting that a lower C p_z band center can strengthen proton binding. Note this is in contrast with the results of proton adsorption onto transition metal surfaces described by the d-band center theory [62], because of the full occupancy of the σ^* orbitals of H* and C when protons are adsorbed on carbon active sites, where few electronic states can be found in the conduction bands (Fig. 3e-f). Therefore, the bonding with proton will be strengthened with a deeper valence orbital levels of the graphitic sheet. From these DFT calculations, one can see that indeed dopants and substrate interactions play an important role in boosting the activity of carbon towards HER by charge transfer from the substrate to carbon.

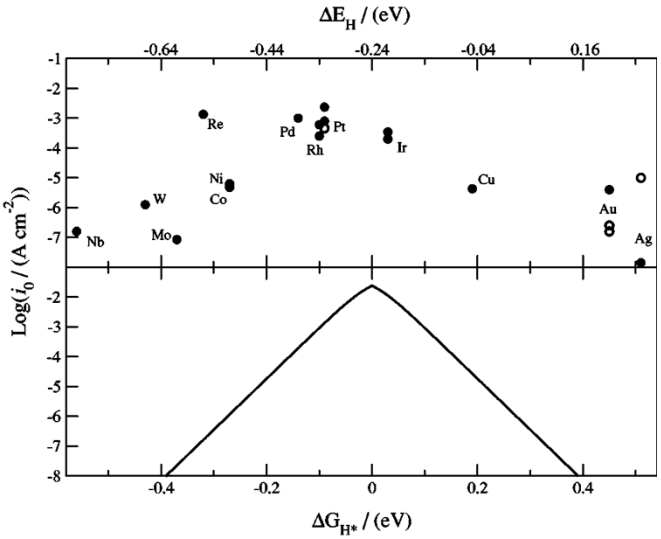

Figure 2. Experimental results of exchange current density (j_0) of HER over different metal surfaces plotted as a function of calculated Gibbs free energy of hydrogen adsorption per atom (ΔE_H, top axis) and the fitted volcano plot as a function of Gibbs free energy of hydrogen adsorption (ΔG_{H^*}). $\Delta G_{H^*} = \Delta E_H$ + 0.24 eV. (Reproduced with permission from Ref. [57] © 2005 The Electrochemical Society)

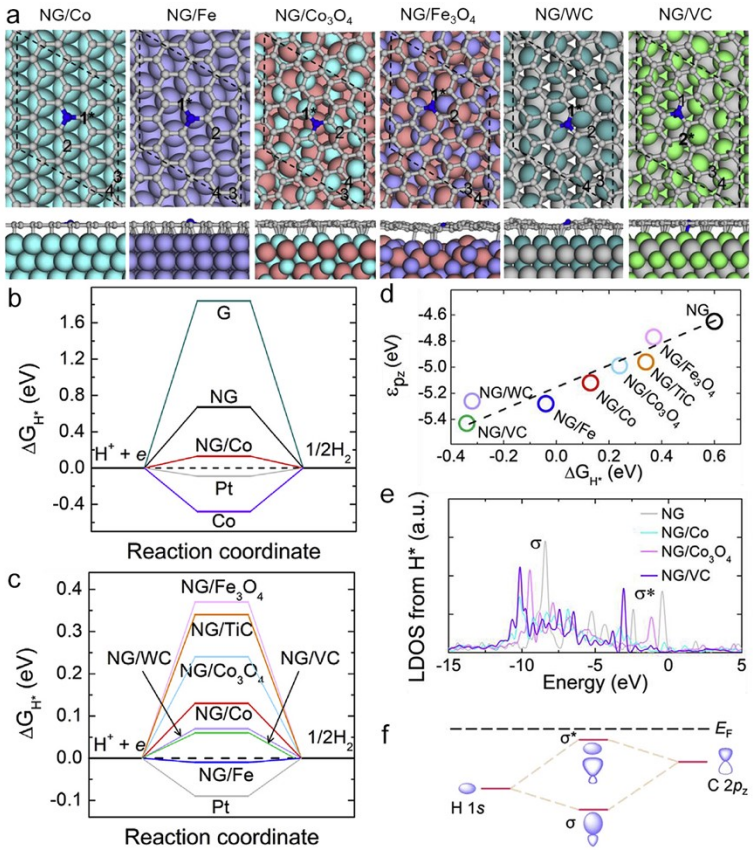

Figure 3. (a) Top and side views of N-doped graphene on various substrates. (b-c) Free energy diagrams for HER at zero potential and pH = 0 on G, NG, Co, NG/Co and Pt surfaces, and NG on various substrates. (d) The plot of C p_z center versus ΔG_{H^*} of different hybrids. (e) LDOS of a H atom adsorbed on the active sites of various hybrids. (f) Schematic illustration of H-C bonds formation on the hybrids. (Reproduced with permission from Ref. [61] © 2018 Elsevier)

Such interfacial charge transfer is also responsible for electrocatalytic activity towards other reactions, such as OER and ORR. Here we will focus on OER [63-67], as ORR is the reverse of OER and has been widely studied [68-72]. Generally, OER in alkaline media involves four steps as described below [65],

$* + OH^- \leftrightarrow HO^* + e^-$	$\Delta G(HO^*)$	(4)
$HO^* + OH^- \leftrightarrow H_2O + O^* + e^-$	$\Delta G(O^*)$	(5)
$O^* + OH^- \leftrightarrow HOO^* + e^-$	$\Delta G(HOO^*)$	(6)
$HOO^* + OH^- \leftrightarrow * + O_2 + H_2O + e^-$	$\Delta G(*)$	(7)

The overall reaction energy $\Delta G^{OER} = \Delta G(HO^*) + \Delta G(O^*) + \Delta G(HOO^*) + \Delta G(*)$, which is a constant. Here we take FeNi@C [35] as an illustrating example. Fig. 4a schematically illustrates a FeNi@C model for DFT calculation and the adsorption of various oxygen intermediates. Fig. 4b plots the Gibbs free energies at different reaction stages under various potentials, from which an overpotential of 0.49 V is suggested to catalyze OER on FeNi@C, as compared to the equilibrium potential (1.23 V). Extending the studies to other M@C samples involving a range of metal nanoparticles (Fig. 4c), one can see that there is a good scaling relationship between $\Delta G(HO^*)$ and $\Delta G(HOO^*)$ with an intercept of 3.2 eV and a slope of 1 [65], indicating that HO* and HOO* likely follow the same bonding mechanism to the catalyst surface. The overpotential can be readily determined by the difference of the binding free energy between O* and HO*, $\Delta G(O^*) - \Delta G(HO^*)$. Using this as an activity descriptor, one can see that the plot of calculated overpotential versus $\Delta G(O^*)$-$\Delta G(HO^*)$ displays a volcano feature (Fig. 4d), and that of FeNi@C is ca. 1.48

eV, closest to the volcano peak, which suggests that FeNi@C is the most active one among the series of samples. This is indeed confirmed by experimental studies. Fig. 4e-f displays the representative TEM and HRTEM images of FeNi@NC, where FeNi nanoparticles of 6-10 nm (with well-defined lattice fringes) are encapsulated within a single layer graphene shell. Electrochemical measurements (Fig. 4g-h) show that the OER performance of the series of M@NC catalysts follows the order of FeNi > CoNi > FeCo > Ni > Co > Fe, by comparing the electrode potentials needed to reach the current density of 10 mA/cm^2 (E_{10}). This is, again, ascribed to electron transfer from the metal core to the carbon shell that manipulates the ΔG of reaction intermediates, specifically, ΔG(O*) – ΔG(HO*). In fact, the number of electrons gained per metal atom is 0.15, 0.12, 0.07 and 0.10 for Fe@C, Co@C, Ni@C and FeNi@C, respectively, where the corresponding ΔG(O*) – ΔG(HO*) increases to 1.03, 1.06, 1.21 and 1.48 eV, as compared to that of pristine graphene. The best sample, FeNi@NC, also shows excellent durability, as compared to the benchmark IrO_2 catalyst when tested at the current density of 40 and 100 mA/cm^2 for 10,000 cycles (Fig. 4h), consistent with results from the DFT calculations.

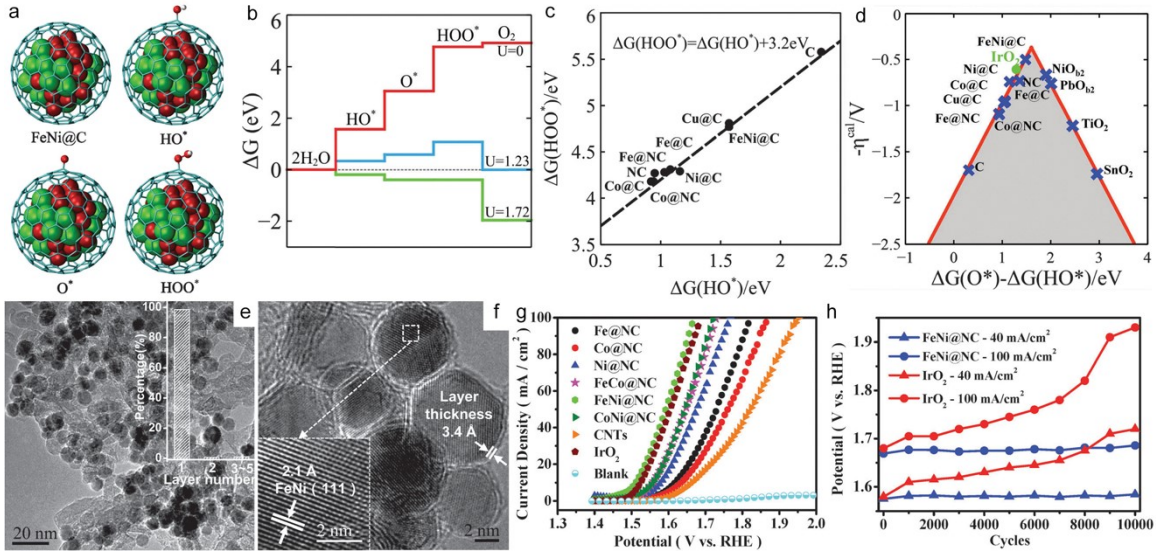

Figure 4. (a) Schematic model of FeNi@NC and OER steps on the catalyst. (b) Free energy profiles for OER on FeNi@C at different potentials. (c) Linear relationship of free energy of HO* (ΔG(HO*)) versus HOO* (ΔG(HOO*)). (d) Overpotential (η^{cal}) based on DFT calculation against the universal descriptor ΔG(O*)-ΔG(HO*). The data of metal oxides were cited from literature [73]. (e) TEM image of FeNi@NC, and inset is the corresponding histogram of the layer number of the graphene shell. (f) HRTEM image of FeNi@NC, and inset is the lattice fringes of FeNi alloy (111) crystalline phase. (g) OER performance of FeNi@NC and other catalysts. (h) Comparison of stability test of FeNi@NC with IrO_2 via potential changes at the constant current density of 40 or 100 mA/cm^2. (Reproduced with permission from Ref. [35] © 2016 Royal Society of Chemistry)

3. Metal core effect

As demonstrated above, interfacial charge transfer from the metal core to the carbon shell is argued to be the main driving force responsible for the electrocatalytic activity of M@C composites. Within this fundamental framework, one can see that the electrocatalytic activity can be readily manipulated by the metal work functions [74, 75], which depends on the chemical nature of the metals (Table 1), as well as elemental composition and arrangement of metal alloys (Table 2). In an early study with metal nanoparticles encapsulated in N-doped graphene (M@NG) [45], the HER activity was indeed found to vary with the elemental composition of the metal nanoparticles. Fig. 5a-c depicts the HRTEM images of RuCo@NG (3.58 wt% Ru), where one can see that the RuCo nanoalloy particles are encapsulated within a carbon shell of 6-15 graphene layers in thickness, and the cubic and hexagonal Co phases can be clearly identified from the lattice fringes, while no Ru phase can be observed due to the low content. Fig. 5d compares the HER performance of the resulting RuCo@NG, Ru nanoparticles, and Pt/C in 1 M KOH. It can be seen that the RuCo@NG sample shows an overpotential (η_{10}) of only –28 mV

to reach the current density of 10 mA/cm^2, a performance even better than that of Pt/C (η_{10} = –40 mV) or Ru nanoparticles (η_{10} = –58 mV). Also, RuCo@NG exhibits great long-term stability since η_{10} only increases by 4 mV after 10,000 cycles, while η_{10} of Pt/C increases by 8 mV and that of Ru nanoparticles increases much more dramatically by almost 70 mV (Fig. 5d). Results from DFT calculations (Fig. 5e) show that $|\Delta G_H^*|$ decreases gradually with the increase of Ru content in $Ru_xCo_{55-x}@N_1C_{239}$ (x = 0, 1, 2, or 3), suggesting that the improved HER performance is likely due to enhanced proton adsorption. Furthermore, from the charge density distribution of $Co_{55}@N_1C_{239}$ and $Ru_3Co_{52}@N_1C_{239}$ (Fig. 5f), the Bader charge transfer number from the metal core to the graphene shell can be estimated to be 5.81 and 5.91, respectively, consistent with the higher HER activity observed with RuCo@NG than with Co@NG, likely due to the strengthening of the C-H bond. Certainly one may notice that in the experimental studies the particles are much larger (~30 nm), and the graphene layers much thicker (6-15 layers). This raises serious questions about the direct correlation between the results from the experimental and theoretical studies. Nevertheless, both results suggest that indeed the encapsulated metal nanoparticles may promote proton adsorption by interfacial charge transfer to the carbon shell. In a more recent study [46], IrCo alloy nanoparticles are encapsulated in N-doped carbon cages at a low Ir content of only 1.56 wt%. Yet the sample shows a better catalytic performance (η_{10} = –24 mV) in 0.5 M H_2SO_4 than Pt/C (η_{10} = –35 mV). Remarkable HER activity has also been observed with PdCo@NC [44, 76], CoRu@NC and NiRu@NC [77, 78]. Such M@C nanostructures have also shown apparent activity towards other reactions, such as ORR, ethanol oxidation reaction, and single cell [43, 79, 80].

Table 1. Summary of electrocatalytic performances of single-metal M@C nanocomposites

Metal core	Carbon shell	Electrolyte	Electrocatalytic Performance†	Ref.
Co	C	1.0 M KOH	Overall water splitting: E_{10ws} = 1.653 V	[81]
Co	Co,N,S-G	1.0 M KOH	HER: η_{10} = –247 mV; OER: η_{10} = +337 mV	[82]
Co	N-C	0.5 M H_2SO_4 (0.1 M NaOH)	HER : η_{10} = –265 mV (–337 mV)	[36]
Co	N-C	0.5 M H_2SO_4 (1.0 M KOH)	HER: η_{10} = –82 mV (–95 mV); ORR: $E_{1/2}$ = 0.78 V (0.9 V)	[37]
Co	N-CNT	0.5 M H_2SO_4	HER: η_{10} = –215 mV	[38]
Co	N-CNT	0.1 M KOH (1.0 M PBS)	OER: η_{50} = 300 mV (η_{10} = 310 mV); ORR: E_{onset} = 0.8 V (0.75 V)	[83]
Cu	N-C	0.1 M KOH	ORR: $E_{1/2}$ = –0.24 V vs SCE, E_{onset} = –0.06 V vs SCE	[84]
Co	B,N-C	0.5 M H_2SO_4 (1.0 M KOH)	HER: η_{10} = –96 mV (–183 mV)	[39]
Ni	G	1.0 M KOH	HER: η_{10} = –240 mV; OER: η_{10} = +370 mV	[85]
Co	N-C/N-rGO	0.1 M KOH	ORR: E_{onset} = 0.94 V; HER: η_{10} = –229 mV; OER: η_{10} = 430 mV	[86]
Co	N-G	0.5 M H_2SO_4 (1.0 M KOH)	ORR: E_{onset} = 0.77 V (0.90 V), $E_{1/2}$ = 0.55 (0.83 V); HER: η_{10} = –183 mV (–220 mV)	[87]
Co	N-C	0.1 M KOH	ORR: E_{onset} = –0.08 V, $E_{1/2}$ = –0.15 V vs Ag/AgCl (3.5 M KCl)	[88]
Co	N-CNT	0.5 M H_2SO_4	HER: η_{10} = –280 mV	[40]
Fe	N-CNT		H_2-O_2 fuel cell: 60% voltage of Pt/C	[89]
Co	N-CNT	universal pH	HER: η_{10} = –103/–337/–204 mV at pH=0/7/14	[90]
Co	N-CNT	0.1 M KOH	ORR: E_{onset} = 0.929 V, $E_{1/2}$ = 0.849 V	[91]
Co	N-CF	0.5 M H_2SO_4	HER: η_{10} = –61 mV	[41]
Co	rGO	0.1 M KOH	ORR: E_{onset} = –0.01 V vs SCE	[92]

Co	N-C/CNT	1.0 M KOH	Overall water splitting: E_{10ws} = 1.625 V	[93]
Co	N-CF	1.0 M KOH	Overall water splitting: E_{10ws} = 1.66 V	[94]
Co	N-G	0.5 M H_2SO_4	HER: η_{10} = –125 mV	[42]
Cu	N-C	0.1 M KOH	ORR: E_{onset} = +0.94 V, $E_{1/2}$ = 0.83 V	[95]
Ni	N-C	1.0 M KOH	HER: η_{20} = –88 mV	[96]
Co	N-CNT	0.1 M KOH	Oxygen electrode: ΔE = 0.78 V	[97]
Co	N-G	0.1 M KOH	ORR: E_{onset} = –0.035 V vs SCE	[98]
Co	N-GR/C	0.1 M KOH	ORR: $E_{1/2}$ = 0.83 V	[99]
Co	N-G	1.0 M $LiClO_4$-DMSO	Li-Oxygen battery: 0.58 V overpotential	[100]
Co	NC@GC	0.1 M KOH	Oxygen electrode: ΔE = 0.64 V	[101]
Co	N-C	0.1 M KOH	Oxygen electrode: ΔE = 0.859 V	[102]
Sn	G	0.1 M $NaHCO_3$	CO_2RR: 21.1 mA/cm^2 at –1.8 V vs. SCE	[103]
Co	N-CNT	0.5 M H_2SO_4 (1.0 M KOH)	HER: η_{10} = –280 mV (–240 mV)	[104]
Au	N-C	0.5 M H_2SO_4	HER: η_{10} = –130 mV	[105]
Au	Zn-Fe-C	0.5 M H_2SO_4 (0.1 M KOH)	HER: η_{10} = –123 mV, ORR: E_{onset} = 0.94V	[106]

† In HER and OER, η_{10} refers to the overpotential needed to reach the current density of 10 mA/cm^2. In ORR, E_{onset} and $E_{½}$ denote onset potential and half-wave potential, respectively. In oxygen electrode, ΔE is the difference between the potential at the OER current density of 10 mA/cm^2 and ORR half-wave potential, i.e., $\Delta E = E_{10,OER} - E_{½,ORR}$. In overall water splitting, E_{10ws} is the cell potential needed for a current density of 10 mA/cm^2. All the potentials are versus to RHE if there is no special notification.

Table 2. Summary of electrocatalytic performances of alloy M@C nanocomposites.

Alloy core	Shell	Electrolyte	Electrocatalytic Performance†	Ref.
PdCo	N-C	0.5 M H_2SO_4	HER: η_{10} = –80 mV	[44]
FeCoNi	N-C	1.0 M KOH	overall water splitting: E_{10ws} = 1.667 V	[107]
FeNi	N-C	1.0 M KOH	overall water splitting: E_{10ws} = 1.63 V; oxygen electrode: ΔE = 0.81 V	[108]
NiCu	GC	universal pH	HER: η_{10} = –48/-164/-74 mV at pH = 0/7/14	[109]
IrCo	N-C	0.5 M H_2SO_4	HER: η_{10} = –24 mV	[46]
NiCo	N-C	0.5 M H_2SO_4	HER: η_{10} = –200 mV	[60]
$Ni_{0.4}Co_{0.6}$	N-C	1.0 M KOH	HER: η_{10} = –68 mV	[110]
NiCo	N-C	0.1 M KOH	ORR: $E_{1/2}$ = 0.81 V	[111]
NiCo	N-CNT	0.1 M KOH	ORR: E_{onset} = 0.93 V, $E_{1/2}$ = 0.82 V	[112]
PtPd	N-G	0.5 M H_2SO_4 (0.1 M KOH)	HER: η_{10} = –58 mV; ORR: E_{onset} = 0.97 V	[113]

CoNi	N-C	0.1 M KOH	ORR: E_{onset} = 0.923 V, $E_{1/2}$ = 0.821 V	[114]
FeCoNi	N-C	0.5 M KOH	OER: η_{10} = 400 mV	[115]
FeCo	N-C	0.5 M H_2SO_4	HER: η_{10} = –262 mV	[116]
CoNi	N-C	1.0 M KOH	OER: η_{10} = 280 mV	[35]
PdCo	N-C	0.1 M KOH	ORR: E_{onset} = 0.914 V	[43]
NiRu	N-C	universal pH	HER: η_{10} = –50/-482/-32 mV at pH = 0/7/14	[77]
NiCo	N-CNT	0.1 M KOH	OER: η_{10} = 410 mV	[117]
NiCo	PFC	0.1 M KOH	Oxygen electrode: ΔE = 0.86 V	[118]
PtCo	N-C	0.1 M $HClO_4$ (0.1 M KOH)	ORR: E_{onset} = 0.929 V (0.925 V)	[80]
NiCo	N-C	1.0 M KOH	Overall water splitting: E_{10ws} = 1.706 mV	[119]
CoRu	N-C	0.5 M H_2SO_4 (1.0 M KOH)	HER: η_{10} = –32 mV (–45 mV)	[78]
RuCo	N-G	1.0 M KOH	HER: η_{10} = –28 mV	[45]
FeCo	N-G/CNT	1.0 M KOH	Water splitting: E_{10ws} = 1.88 V	[120]
FeCo	N-C-KB	0.5 M H_2SO_4	ORR: E_{onset} = 0.92 V, $E_{1/2}$ = 0.74 V; HER: η_{10} = –240 mV	[121]

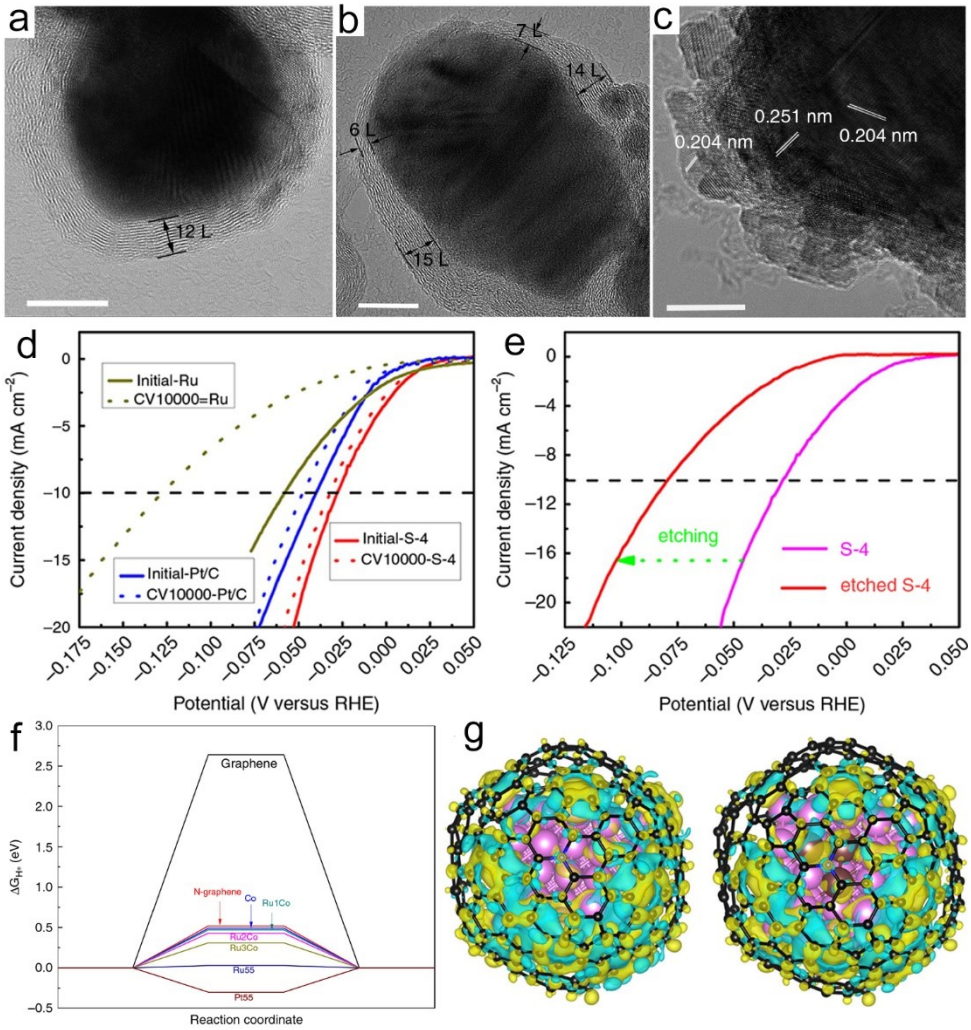

Figure 5. (a-c) HRTEM images of RuCo@NG catalyst. Scale bar 10 nm. (d) Polarization curves of HER catalyzed by RuCo@NG (labelled "S-4"), Ru nanoparticles, and Pt/C in 1 M KOH in the first and 10000th potential cycles. (e) Effect of 1 M HCl etching on the HER catalytic performance of RuCo@NC. (f) DFT calculated HER free energy diagram. (g) DFT calculated charge-density differences of $Co_{55}@N_1C_{239}$ and $Ru_3Co_{52}@N_1C_{239}$ models. The isosurface value of the color region is 0.01 e·Å^{-3}. The yellow and cyan regions refer to increased and decreased charge distributions, respectively. (Reproduced with permission from Ref. [45] © 2017 The Authors)

Further enhancement of the electrocatalytic performance can be achieved by incorporating a third metal forming more complicated alloy nanoparticles in the catalysts. In an earlier study [107], Yang et al. prepared a series of binary and ternary alloy nanoparticles encapsulated in N-doped carbons and compared the OER and HER activities. Fig. 6a shows a representative HRTEM image of a single FeCoNi@NC nanoparticle embedded within a NC matrix of ca. 1.71 nm in thickness and the elemental composition is confirmed in the corresponding STEM elemental mapping analysis (Fig. 6b$_1$-b$_4$). The OER performance was evaluated in 1.0 M KOH, and the results (Fig. 6c) show that within the context of E_{10}, most of the prepared samples exhibited a better activity than commercial RuO_2, and FeCoNi-2 (prepared at the initial feed ratio of Fe:Co:Ni = 3:4:3) stood out as the best among the series. For HER, the performance varied in the order of Pt > FeCo > FeCoNi-1 (Fe:Co:Ni = 4:4:2) > FeCoNi-2 > FeCoNi-3 (Fe:Co:Ni = 2:4:4) > CoNi > FeNi > Co (Fig. 6d). This suggests that the OER and HER activity can be readily adjusted by the elemental compositions of the metal alloy cores. DFT calculations based on a 55-atom metal cluster (Fig. 6e) show that (i) ΔG_{H^*} followed the same order as the experimental results, where the best catalyst FeCo exhibited the lowest ΔG_{H^*} (Fig. 6f), (ii) the calculated volcano plot (Fig. 6g) of OER

suggested that the OER activity could be improved by incorporating multiple metals into the core and increasing the degrees of freedom of the alloys. Fig. 6h depicts the Bader charge transfer profiles of the various M@C structures, and the numbers of electron transfer were estimated to be 5.81, 6.69, 6.50 and 5.25 for M = Co, FeCo, FeCONi and CoNiFe, respectively. Therefore, one can see that the composition of the metal core can indeed efficiently affect the electronic structure of the graphene shell, a unique feature that can be exploited to tailor the catalytic activity towards different reactions.

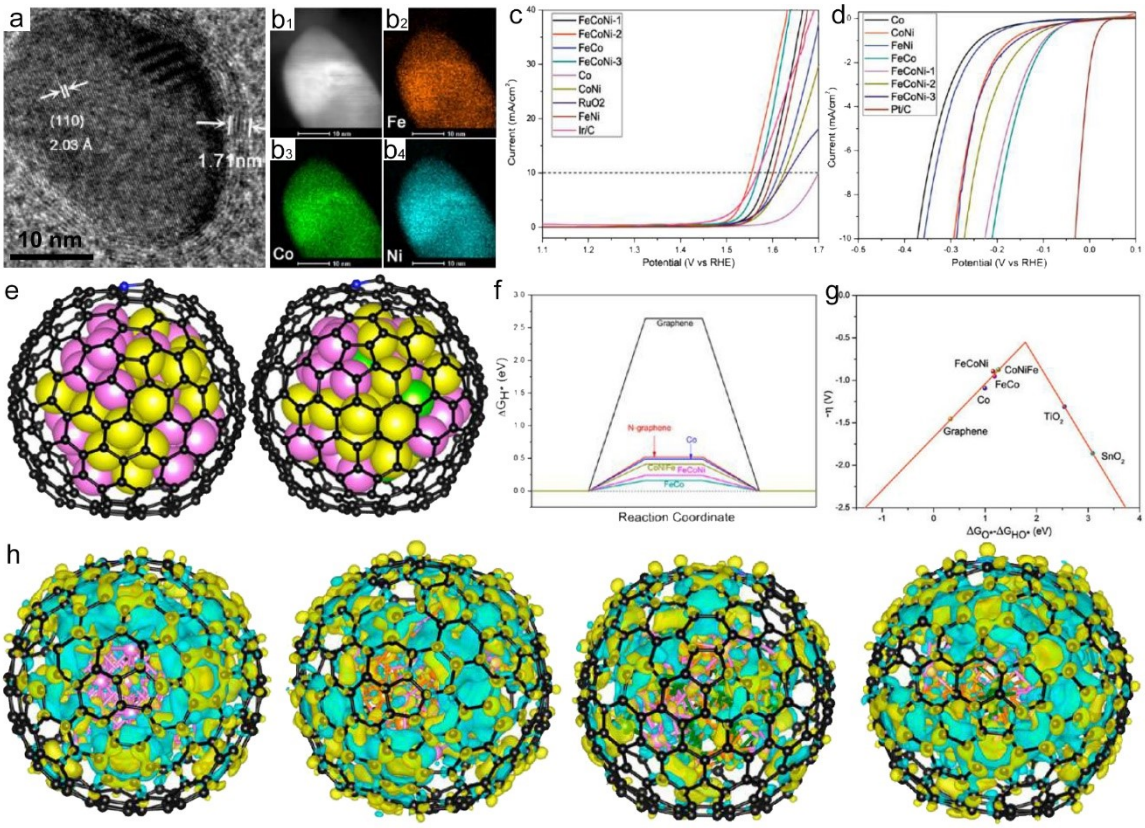

Figure 6. (a) Representative TEM image of FeCoNi@NC. (b) STEM images of a single FeCiNi alloy nanoparticle and the corresponding elemental maps of Fe, Co, and Ni. (c) OER and (d) HER polarization curves of various M@NC catalysts in 1.0 M KOH. (e) Schematic models of M@NG hybrids. Left: FeCo@NG; Right: FeCoNi@NG, and the corresponding ΔG_{H^*} is shown in panel (f), whereas the calculated overpotential of OER versus ($\Delta G(O^*)$-$\Delta G(HO^*)$) is plotted in panel (g). (h) Calculated charge density difference of various M@C models (the core structures from left to right are Co, FeCo, $Fe_{24}Co_{24}Ni_7$, and $Fe_{15}Co_{20}Ni_{20}$, respectively). The isosurface value is 0.01 e/Å^3, and yellow and cyan regions represented the increase and decrease of charge distributions, respectively. (Reproduced with permission from Ref. [107] © 2016 American Chemical Society)

4. Carbon shell effect

For M@C catalysts, reactions occur on the carbon shell surface. Thus, one can envisage that the electrocatalytic performance can also be readily manipulated by the structure of the carbon shell. One effective strategy is to dope the carbon materials with select heteroatoms [122-125]. Notably, for undoped carbon, the electrocatalytic performance is generally subpar [81, 85, 92, 103, 109, 115, 126]. For instance, in ORR, the onset potential (E_{onset}) of Co nanoparticles encapsulated in undoped carbon (Co@C) was 50 mV more negative than that of Pt/C; yet when the carbon was doped with nitrogen, the performance was actually better than that of Pt/C [88, 92, 101]. In some other studies [85, 93, 94, 119], the performance of overall water splitting by Ni@C was found to be markedly enhanced with a doped carbon shell, as compared to that with undoped carbon. In fact, experimentally, a wide range of dopants, including nonmetal elements and metal elements (Tables 1 and 2) have been incorporated into the C shell. For

instance, the Ye group [39] prepared Co@C for HER electrocatalysis, where the carbon shell was doped by N alone or co-doped by N and B. Fig. 7a depicts the polarization curves of a series of Co@C electrocatalysts, from which the η_{10} values can be identified at −284, −191, and −96 mV for Co@C, Co@NC and Co@BNC, respectively, suggesting that doping of the carbon shell indeed enhanced the HER activity, and the enhancement was more pronounced with dual doping than with mono-doping. To unravel the mechanistic origin, DFT calculations were carried out by using a $Co_{55}@C_{240}$ model, where a select number of C atoms were replaced by N and/or B. The ΔG_{H^*} results are plotted in Fig. 7b. One can see that the undoped carbon shell shows a very positive ΔG, indicative of difficult H* adsorption, while the ΔG of the metal core is very negative, suggesting strong proton adsorption. Again, the formation of M@C composites led to a markedly reduced ΔG_{H^*} to 0.35 eV [57]. Interestingly, doping led to a further decrease of the ΔG_{H^*} to 0.23 eV for the $C_{234}N_6$ shell and even lower to 0.118 eV for the $C_{232}N_6B_2$ shell. This is contributed to charge transfer from the metal core to carbon shell and more importantly the introduction of an asymmetrical spin and charge density by doping of N and B due to their electronegativity difference, leading to the formation of more C and N as active sites for HER (Fig. 7c). In another study [89], Fe nanoparticles were encapsulated in N-doped Pod-like carbon nanotubes (Pod(N)-Fe) and used as ORR electrocatalysts. The resultant Pod(N)-Fe or Pod(N)-FeCo exhibited enhanced ORR activity, as compared to Pod-Fe with undoped CNT (Fig. 7d). DFT calculations using the models of Fe_4@SWCNT and Fe_4@N-SWCNT (Fig. 7e) show that based on the p-DOS of the p-orbital of Fe_4-bonded C and the charge density difference, N-doping increased the DOS near the Fermi level and reduced the work function of the surrounding area, as compared to that without N-doping. Fig 7f displays the corresponding ORR free energy diagrams. One can see that after N-doping, the oxygen adsorption free energy deceased to −0.4 eV from +0.03 eV without N-doping, indicating that N-doping efficiently facilitated oxygen adsorption and the associative pathway to convert O_2 to H_2O. Overall, results from these studies demonstrate that dopants in the carbon shell have two major effects: to further manipulate the electronic structure of the surrounding atoms by charge transfer interactions; and to promote the formation of additional active sites.

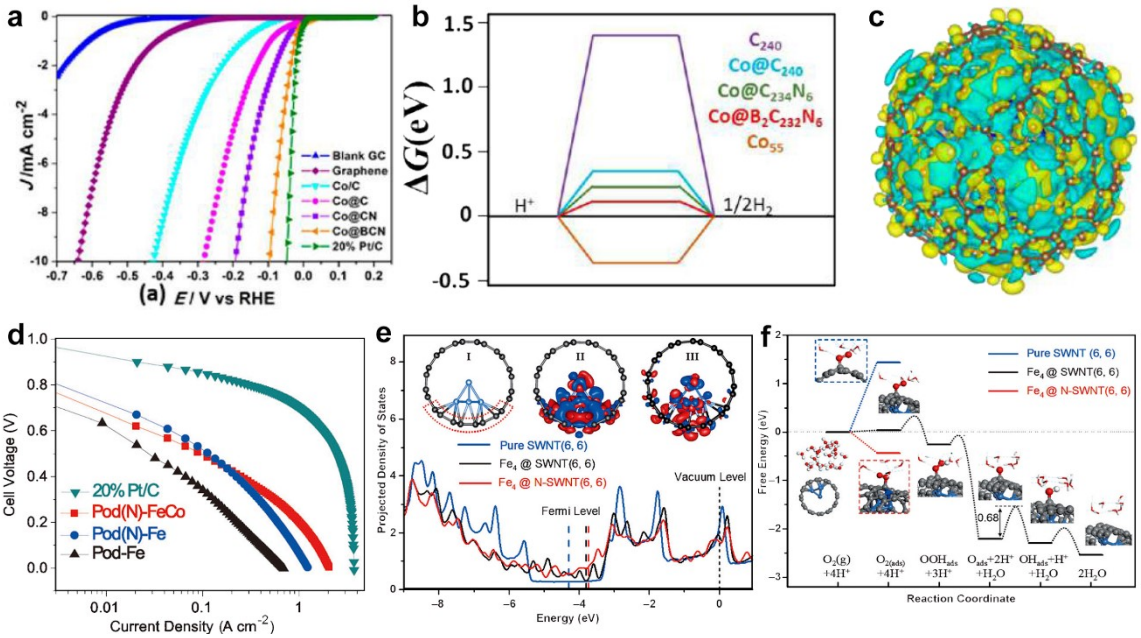

Figure 7. (a) HER polarization curves of a series of M@C catalysts in 0.5 M H_2SO_4. (b) DFT calculated ΔG_{H^*} on different HER electrocatalysts. (c) Charge density difference of the $Co_{55}@C_{232}N_6B_2$ model. The isovalue is 0.0006 e/A^3. Yellow and cyan are charge accumulation and depletion with respect to an isolated Co_{55} core and $C_{232}N_6B_2$ shell. (d) Single H_2-O_2 fuel cell performance tests with different cathode catalysts. (e) DFT calculated p-DOS of the p orbitals of C atoms in SWCNT or C atoms bonding to a Fe_4 cluster in Fe_4@SWCNT and Fe_4@N-SWCNT. Inset: I and II are the relaxed structures of Fe_4@SWCNT and the corresponding charge density difference; III is the charge density difference of Fe_4@N-SWCNT. The red and blue regions represent charge accumulation and depletion, respectively. (f) ORR free energy diagrams on various electrocatalysts. (a-c: Reproduced with permission from Ref. [39] © 2015 American

Chemical Society. d-f: Reproduced with permission from Ref. [89] © 2013 Wiley-VCH)

The electrocatalytic activity of M@C also depends on the thickness of the carbon shell. For instance, the Bao group [127] carried out DFT calculations to study the effect of the number of CNT or N-CNT layers on the electrocatalytic activity of Fe_4@CNT and Fe_4@N-CNT. As shown in Fig. 8a, the dissociative adsorption energies of oxygen ($E_{a(dis)}$) increased almost linearly with the number of CNT layers increased from 1 to 3 for both Fe_4@CNT and Fe_4@N-CNT. Note that a smaller $E_{a(dis)}$ is expected for better ORR catalysts. In addition, the difference of the catalytic performance between CNT and Fe_4@CNT or between N-CNT and Fe_4@N-CNT diminished with the increase of the carbon nanotube layers, and the difference almost vanished when the number of nanotube layer reached 3, indicating that the effect of the metal cores now became negligible and the catalysts behaved equivalently to metal-free carbon alone [122-125]. In another study with Cu@NC [84], DFT calculations showed that charge transfer occurred from the Cu cores to the single layer NC shell, leading to manipulation of the adsorption energy of O_2 on the NC shell (Fig. 8b). However, for a shell of 2 NC layers (Fig. 8c), the electronic interactions were mainly between Cu core and the internal NC shell but not the external one. This apparently contradicts the experimental results described above. One possible reason is that in experimental study, the prepared M@C composites actually entail a range of carbon shell thicknesses; yet it is technically challenging to resolve a single carbon layer on metal nanoparticle surface that make dominant contributions to the electrocatalytic activity.

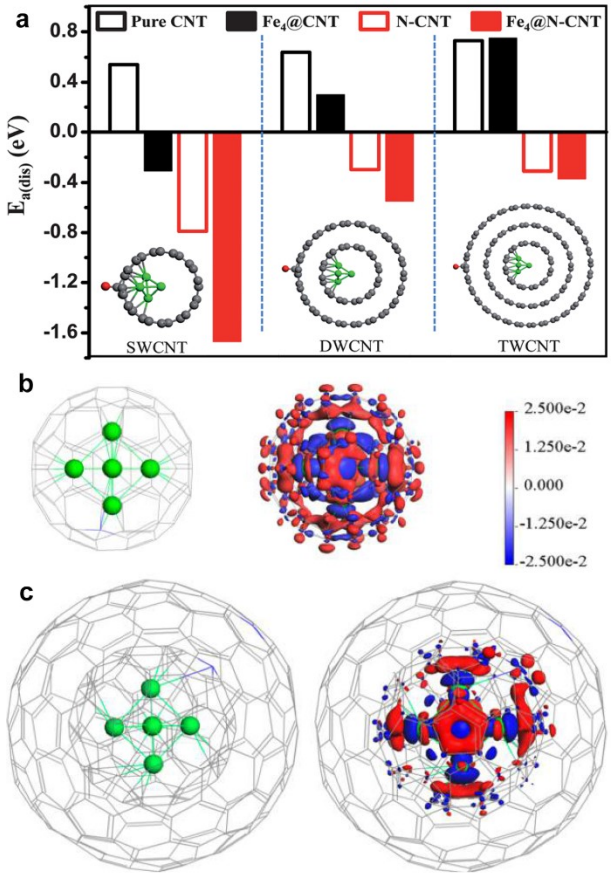

Figure. 8. (a) Dissociative adsorption energy of oxygen on the surface of various ORR catalyst models including CNT, N-CNT, Fe_4@CNT and Fe_4@N-CNT, where the number of CNT layer varies from 1 to 3. Models of Cu@NC with (b) 1 NC layer or (c) 2 NC layers, and the corresponding charge density differences. The red and blue regions represent the charge accumulation and depletion, respectively. (a: Reproduced with permission from Ref. [127] © 2013 Royal Society of Chemistry; b-c: Reproduced with permission from Ref. [84] © 2017 American Chemical Society)

The impacts of the thickness of the carbon shell have also been observed in HER electrocatalysis.

For instance, Deng et al. [60] compared the HER activity of NiCo@NC for HER with CoNi nanoalloys of 4-7 nm in diameter encapsulated in a NC shell varied from 1 to 3 graphene layers by controlled pyrolysis at different temperatures (Fig. 9a-b). HER polarization curves (Fig. 9c) showed that the CoNi@NC prepared at 475 °C possessed the best HER catalytic activity among the series of samples except for Pt/C. Fig. 9d plots the ΔG_{H^*} difference between CoNi@NC and NC ($\Delta\Delta G_{H^*}$) and the electronic potentials from DFT calculations as a function of the number of NC layers. It can be clearly seen that with an increasing number of the NC layers from 1 to 3, the $\Delta\Delta G_{H^*}$ decreased from 0.8 eV to 0.1 eV while the electronic potential decreased from -0.5 eV to 0 eV, suggesting that an increase of the NC layer thickness diminished the effect of the CoNi cores on the HER activity, and when the thickness was equal to or greater than 3 layers, there was virtually no effect. The charge density difference profiles of CoNi@NC with 1-3 NC layers (Fig. 9e) also suggest that whereas electron transfer occurred from the CoNi core to the NC layers, it decreased dramatically with the NC layer thickness.

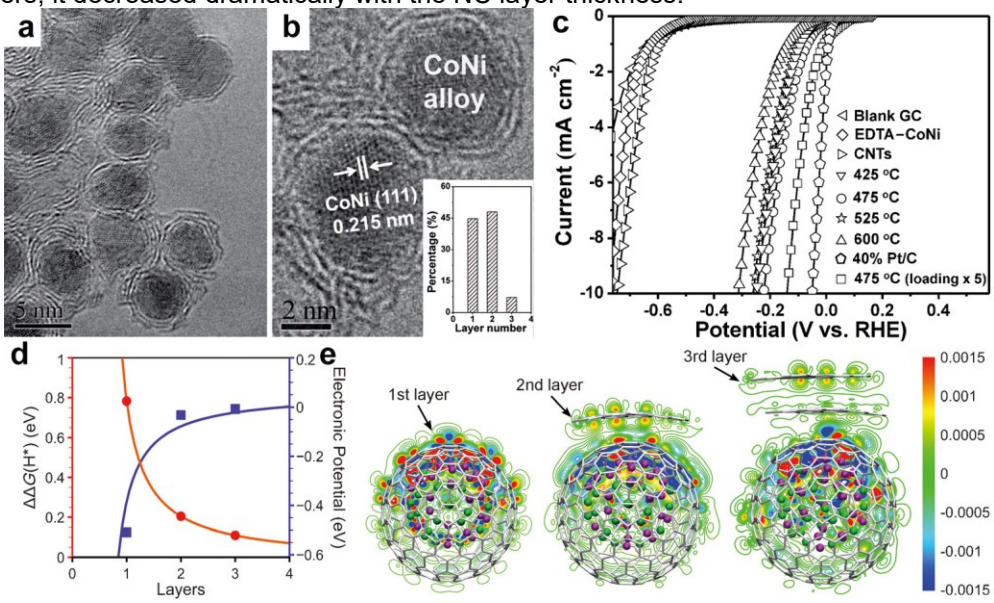

Figure 9. (a-b) TEM and HRTEM images of CoNi@NC. Inset to (b) is the histogram of the number of NC layers. (c) HER polarization curves of a series of electrocatalysts measured in 0.5 M H_2SO_4. (d) ΔG_{H^*} difference between CoNi@NC and the NC shell ($\Delta\Delta G_{H^*}$) and electronic potential vs. the number of NC layers. (e) Charge density difference of CoNi@NC with 1-3 NC layers. The red and blue regions represent charge accumulation and depletion, respectively. (Reproduced with permission from Ref. [60] © 2015 Wiley-VCH)

These studies clearly demonstrate that the number of graphene layers exhibits significant impacts on the electronic structure of the M@C nanostructures. Yet charge transfer from the metal cores to the carbon shell is primarily confined to the first three graphene layers. In most prior experimental studies, the M@C catalysts primarily entail a much thicker carbon shell. This suggests that one should be critical in developing a relevant structural model for theoretical simulations and calculations, such that the theoretical insights may be directly correlated with the experimental data to account for the electrocatalytic performance and, more importantly, to unravel the mechanistic origin. Meanwhile, it is highly desired to develop effective synthetic protocols for ready control of the carbon shell thickness, in which some progress has been made [35, 128].

5. Third component effect

The electrocatalytic performance of M@C nanostructures can also be manipulated by a third component that is typically incorporated as part of the core or shell, or hybridized with the M@C composites. Such third components typically entails metal oxides, such as TiO_2 [129], CoO [61, 130], Co_3O_4 [91, 98, 131] and $MM'O_x$ (M, M' = Fe, Co, Ni, and Cu) [132-134], and can be used as

multifunctional electrocatalysts towards ORR, OER and HER. For instance, the Sun group [132] prepared CuCo/$CuCoO_x$@NC hybrids as bifunctional electrocatalysts for overall water splitting, where a cell voltage (E_{10ws}) of only 1.53 V was needed to reach a 10 mA/cm^2 current density, and claimed that one of the contributions was from the metal-semiconductor Mott-Schottky structure which optimized charge transfer in the material [135, 136]. Jin et al. [130] prepared Co/CoO_x@NC as HER and OER bifunctional catalysts and found that the presence of Co^{2+} enhanced the OER performance via a synergetic interaction between the cobalt metal and cobalt oxides. In another study, Yu et al. [129] examined the HER activity of Co@NCNT, and found that hybridization with defective TiO_2 (D-TiO_2/Co@NCNT) led to marked enhancement of the HER performance. The structure of the D-TiO_2/Co@NCNT hybrid was first characterized by TEM measurements (Fig. 10a-b), and the structural defects of TiO_2 were confirmed by XPS measurements where a Ti^{3+} peak was identified at 455.2 eV (Fig. 10c), and EPR measurements that showed a stronger radical O^{2-} signal at g = 2.00 in D-TiO_2/Co@NCNT than in TiO_2-NC (Fig. 10d). Impressively, the resulting D-TiO_2/Co@NCNT composite exhibited an excellent HER activity with a low η_{10} of −167 mV (Fig. 10e) and a small Tafel slop of 73.5 mV/dec (Fig. 10f). DFT calculations based on a relaxed model of defective TiO_2 with one O vacancy (Fig. 10g) showed that ΔG_H at the Ti defect site was only 0.081 eV, comparable to that of state-of-the-art catalysts Pt/C (ΔG_{H^*} = −0.09 eV), indicating that the D-TiO_2 provided additional active sites for HER.

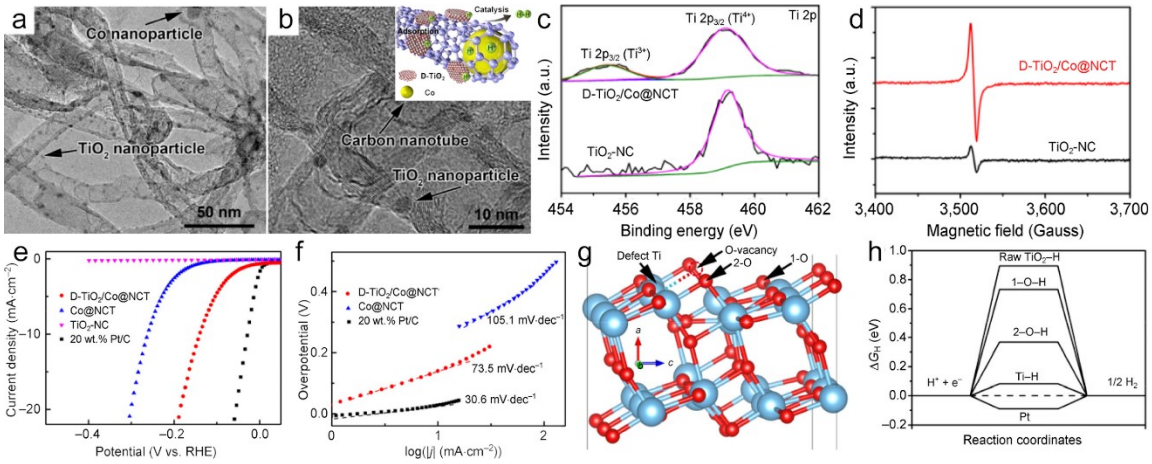

Figure 10. (a-b) TEM images of D-TiO_2/Co@NCNT. Inset to (b) is a structural schematic. (c) XPS and (d) EPR spectra of Ti 2p in D-TiO_2/Co@NCNT and TiO_2-NC. (e) HER polarization curves of different electrocatalysts in 0.5 M H_2SO_4 electrolyte, and (f) the corresponding Tafel plots. (g) Atomic model of TiO_2 with one O vacancy after relaxation. (h) Calculated ΔG_{H^*} at different sites in the model. (Reproduced with permission from Ref. [129] © 2017 Tsinghua University Press and Springer-Verlag Berlin Heidelberg.)

In another study [137], the Chen group prepared Fe/Fe_3C@NC nanorods, where the cores were Fe/Fe_3C composite rods and the shells were N-doped graphene, and observed improved ORR activity in neutral electrolytes, as compared to commercial Pt/C. They then successfully used Fe/Fe_3C@NC as cathode catalysts for microbial fuel cells. In a further study [138], they developed a more complex structure consisting of Fe/Fe_3C@C nanoboxes on reduced graphene oxide (rGO), which exhibited apparent ORR activity in alkaline electrolyte. More recently, Wang et al. [139] synthesized Fe/Fe_3C nanoparticles encapsulated in a N-doped graphene-CNT framework, which exhibited bifunctional activity towards both ORR and OER, and thus was used as oxygen electrodes in rechargeable Zn-air batteries. However, the role of Fe_3C in the structures remained unknown, since no control experiments were included to examine and compare the activity of Fe@NC [89, 140].

Separately, the Lou group [91] embedded Co nanoparticles within a carbon matrix and encapsulated the composites with a Co_9S_8 shell. They found the Co_9S_8 layer led to the generation of an increasing number of ORR active sites and hence enhanced ORR performance, as compared to that without the overlayer [83, 88, 91, 92, 99, 102, 141]. A variety of composite catalysts were prepared in a similar fashion, such as Fe_3O_4/Co_9S_8/rGO, Co/Co_9S_8/C, and Co/Co_9S_8/SN-C [142-144]. For instance, Hao et al. [145] embedded Co/CoP in N-doped carbon as tri-functional electrocatalysts for ORR, OER and

HER, a unique feature for applications like water splitting and rechargeable metal-air battery. This is due to the addition of CoP that led to the formation of more active sites [146-148]. Furthermore, Jin et al. [149] prepared Co@C/$Co(OH)_2$ composites for HER electrocatalysis, where $Co(OH)_2$ was in-situ formed by an electrochemical treatment.

These representative examples highlight the unique strategies in the design and engineering of high-performance (multi-functional) catalysts by the incorporation of a third component, due to the following advantages: (i) generation of additional catalytic active sites, (ii) further control of the electronic properties of the M@C nanostructures due to synergetic interactions between the third component and M@C, and (iii) applications as multi-functional catalysts.

6. Morphology effect

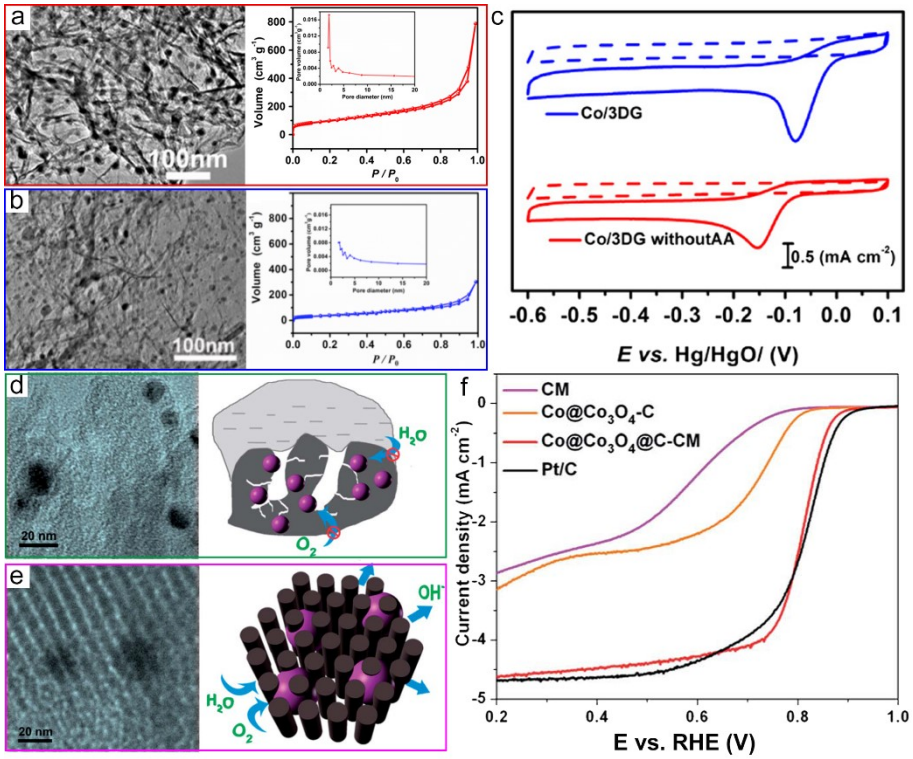

Figure 11. (a-b) TEM image of Co@3DG (a) with and (b) without ascorbic acid treatment, and the corresponding N_2 adsorption-desorption isotherms and pore size distributions (insets). (c) CV curves of the electrocatalysts recorded in N_2 and O_2 saturated 0.1 M KOH. (d-e) TEM images of (d) disordered and (e) ordered Co@Co_3O_4@C, and the corresponding mass transport pathways during ORR. (f) ORR polarization curves of the various catalysts in 0.1 M KOH. (a-c: Reproduced with permission from Ref. [92] © 2017, Springer-Verlag GmbH Germany; d-f: Reproduced with permission from Ref. [150] © 2015 The Royal Society of Chemistry)

In catalyst design, morphology is another important factor that needs to be taken into consideration besides the structural parameters discussed above. For instance, Chen et al. [92] encapsulated Co nanoparticles within 3D graphene (Co@3DG), and found that after ascorbic acid treatment, the sample exhibited enhanced ORR activity. From the TEM images in Fig. 11a-b, one can clearly see that ascorbic acid treatment did not change the 3D structures with Co nanoparticle wrapped inside except that more graphene wrinkles were formed. From the corresponding nitrogen adsorption-desorption isotherms, the BET surface area of Co@3DG was found to be markedly enhanced after acid treatment (ca. 348 m^2/g), due to the generation of an increasing number of mesopores and macropores. In cyclic voltammetric measurements, after acid treatment, Co@3DG possessed a more positive ORR peak potential at −0.08 V (vs. Hg/HgO) and higher cathodic current density of 2.25 mA/cm^2 than the one without acid treatment (ORR peak potential -0.15 V, and peak current density 1.5 mA/cm^2) in 0.1 M KOH electrolyte (Fig. 11c). In another study [150], the Guo group studied and compared the ORR activity of

Co@Co_3O_4@C, where the carbon shell was either a highly ordered porous carbon matrix or disordered porous carbon matrix (Fig. 11d-e). Interestingly, the ordered sample (Co@Co_3O_4@C-CM) showed a much higher ORR activity (E_{onset} = +0.93 V and $E_{½}$ = +0.81 V) than the disordered counterpart (Co@Co_3O_4-C, E_{onset} = +0.85 V and $E_{½}$ = +0.70 V). In fact, the ORR performance of the former is close to that of Pt/C in O_2-saturated 0.1 M KOH (Fig. 11f). This is accounted for by the fact that the ordered open space could better facilitate rapid mass transfer of the gas and electrolyte, which was further confirmed by studies with other catalysts [151, 152]. Indeed, the morphology of the M@C composites can have significant effects on both the electron transfer and mass transport dynamics of the catalytic reactions, and thus is an important factor in catalyst design and engineering [153-156].

7. Applications

In addition to HER, OER and ORR, M@C nanocomposites have also shown potential applications towards other important reactions such as CO_2RR. For instance, the Xie group [103] synthesized graphene confined Sn quantum dots (SnQD@G) using a two-step approach (Fig. 12a). HRTEM measurements (Fig. 12b) suggested that the SnQD was wrapped and well dispersed in the graphene matrix, and AFM study (Fig. 12c) showed that the SnQD exhibited a 2D sheet-like feature with a thickness of ca. 1.41 nm. Interestingly, the SnQD@G sample exhibited a higher catalytic activity towards CO_2RR in CO_2-saturated 0.1 M $NaHCO_3$ than Sn nanoparticles, bulk Sn or the mixture of Sn nanoparticles and graphene (Fig. 12d). Fig. 12e depicts the CO_2 reduction products at various overpotential and the SnQD@G sample showed a higher faradaic efficiency for formate production than other catalysts in the series, which reached a maximum at −1.8 V. This may be due to the high electrochemical surface area of SnQD@G, as manifested in the double-layer capacitance (Fig. 12f). Consistently, the CO_2 adsorption capacity of the SnQD@G catalyst reached 26.1 mg/g at 1 atm, which was 9, 2 and 1.75 times that of bulk Sn, Sn nanoparticles and mixture of Sn nanoparticles and graphene, respectively, as shown in Fig. 12g.

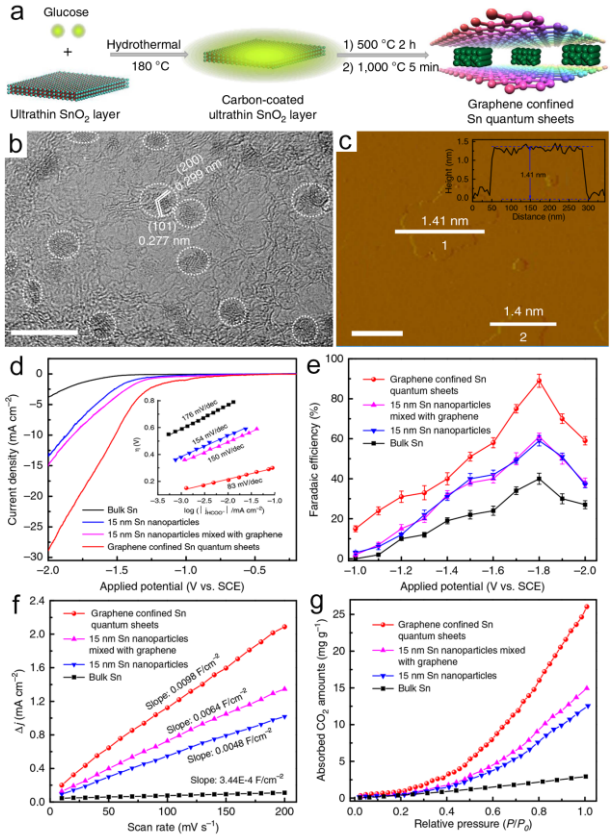

Figure 12. (a) Schematic illustration for the synthesis of SnQD@G. (b-c) HRTEM image (b) and AFM image (c) of SnQD@G. (d) LSV curves recorded in 0.1 M $NaHCO_3$ aqueous electrolyte with various

CO_2RR catalysts, and (e) the corresponding Faradaic efficiency for formate production under different overpotentials. (f) Double-layer capacity derived from the plot of voltammetric current density versus scan rates. (g) CO_2 adsorption isotherms. (Reproduced with permission from Ref. [103] © 2017 The Authors)

Additionally, one of the advantages of M@C nanocomposites is the multi-functional activity that are critical in the applications of, for instance, overall water splitting [13-15] which requires the electrocatalysts to be active for both OER and HER and rechargeable metal-air batteries [16-18] where active electrocatalysts are needed for both ORR and OER. Here we highlight the applications of two M@C catalysts in these electrochemical devices, with additional examples listed in Tables 1 and 2. In one study, Zhao et al. [94] prepared Co nanoparticles embedded in porous N-doped carbon fibers (Co@NC, Fig. 13a-b), which exhibited apparent activity for both OER (E_{10} = +1.515 V, Fig. 13c) and HER (η_{10} = −0.249 V, Fig. 13d) in 1.0 M KOH. Using the Co@NC as both cathode and anode catalysts for overall water splitting in 1.0 M KOH, the authors observed an E_{10ws} value of only 1.66 V, and there was almost no current loss after 10 h's continuous operation at this cell voltage (Fig. 13e-f). In another study [101], Wang et al. prepared Co@NC@GC hybrids (Fig. 14a-b). The sample showed bifunctional catalytic performance towards ORR and OER, with an ORR $E_{½}$ of +0.93 V, 40 mV more positive than that of commercial Pt/C, and OER E_{10} of +1.57 V, as compared to that (+1.59 V) for Ir/C (Fig. 14c-d). That is, the overall potential for the oxygen electrode was only 0.64 V, which was much smaller than leading results in recent literatures [157-160]. With the unique bifunctional characteristics, the catalysts were used as electrode materials for rechargeable Zn-air battery (Fig. 14e). Fig. 14f compares the battery performance with that using commercial Pt/C as electrode catalysts. One can see that Co@NC@GC needed ca. 0.95 V to drive a 5 mA/cm^2 charge/discharge current density, which was lower than that of Pt/C (1.10 V).

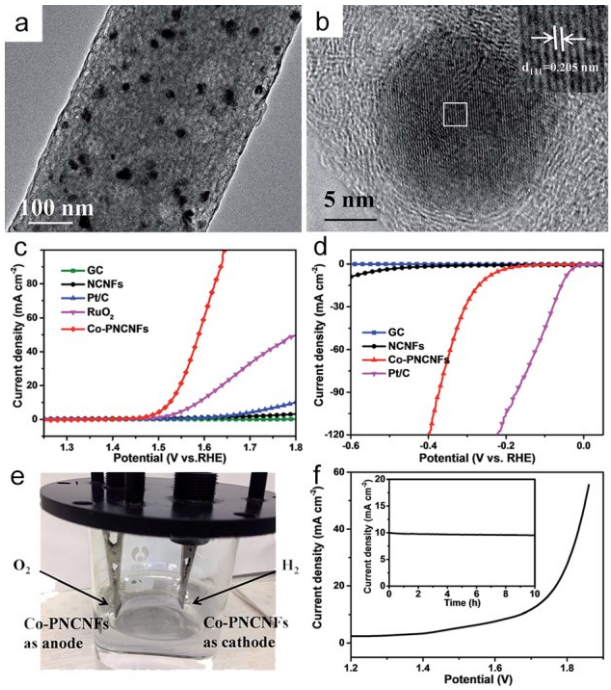

Figure 13. (a-b) TEM image of a single carbon fiber with embedded Co nanoparticles (Co-PNCFs). (c-d) (c) OER and (d) HER polarization curves of Co-PNCFs in 1.0 M KOH, in comparison with other catalysts. (e-f) Photograph of a water splitting cell using Co-PNCNFs as both anode and cathode catalysts, and (f) the corresponding LSV curve. Inset to (f) is the stability test at the potential of 1.66 V over 10 h. (Reproduced with permission from Ref. [94] © 2016 The Royal Society of Chemistry)

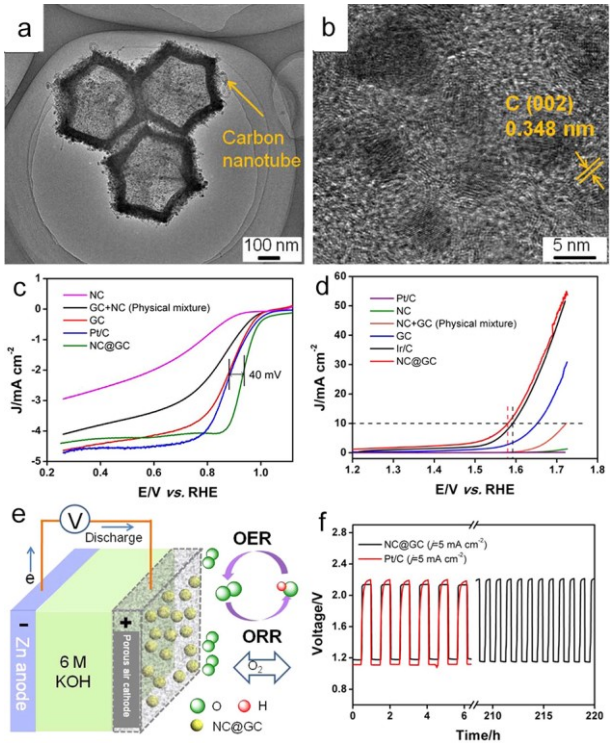

Figure 14. (a-b) TEM images of Co@NC@GC. (c-d) Polarization curves of various electrocatalysts for (c) ORR and (d) OER in 0.1 M KOH. (e) Schematic of a rechargeable Zn-air battery. (f) Cycling performance of a Zn-air battery using Co@NC@GC or Pt/C as electrocatalysts at 5 mA/cm^2. (Reproduced with permission from Ref. [101] © 2016 Elsevier)

8. Summary and perspectives

In summary, M@C core@shell nanocomposites have emerged as a new class of functional nanomaterials that may be exploited as high-performance electrocatalysts towards diverse reactions, due to charge transfer from the metal core to the carbon shell. This synergistic interaction can be readily manipulated by the chemical nature and structure of the metal core (elemental composition, core size, etc) as well as the carbon shell (doping and layer thickness). Further manipulation of the catalytic performance can be achieved by surface morphologies and integration of a third component into the composites, as manifested in a range of studies involving reactions such as ORR, OER, HER and CO_2RR.

In a number of studies that combine theoretical and experimental results, the structural models for theoretical simulations are generally oversimplified. This raises a significant question about the relevance between the two results. In particular, theoretical studies have shown that charge transfer from the metal cores to the carbon shell is primarily confined to the first graphene layer and diminishes sharply with increasing graphene layer thickness, and virtually no impacts are observed with a carbon shell of three or more graphene layers. By contrast, most experimental samples show a much thicker carbon shell. This is likely due to the dispersity of the carbon layer thickness in the samples, and it is a technical challenge to resolve carbon shells of only a few graphene layers. Therefore, a knowledge gap remains in the direct correlation between the experimental and theoretical results. Development of experimental protocols to prepare M@C with a well-defined number of graphene layers is highly desired.

Nevertheless, one can see that the electrocatalytic performance of M@C is apparent and should be of interest in a wide range of important applications, such as full water splitting and metal-air batteries, thanks to the multifunctional activity that can be readily tuned by the composite structures. Promising progress has indeed been made along this line. Continuing research is desired to further improve and eventually optimize the catalytic performance.

Acknowledgment

The authors thank the National Science Foundation (CHE-1710408) for partial support of the work.

References

[1] M. Shao, Q. Chang, J.P. Dodelet, R. Chenitz, Recent advances in electrocatalysts for oxygen reduction reaction, Chem Rev, 116 (2016) 3594-3657.
[2] J. Wang, F. Xu, H. Jin, Y. Chen, Y. Wang, Non-Noble Metal-based Carbon Composites in Hydrogen Evolution Reaction: Fundamentals to Applications, Adv Mater, 29 (2017) 1605838.
[3] D.D. Zhu, J.L. Liu, S.Z. Qiao, Recent Advances in Inorganic Heterogeneous Electrocatalysts for Reduction of Carbon Dioxide, Adv Mater, 28 (2016) 3423-3452.
[4] J. Qiao, Y. Liu, F. Hong, J. Zhang, A review of catalysts for the electroreduction of carbon dioxide to produce low-carbon fuels, Chem Soc Rev, 43 (2014) 631-675.
[5] N.T. Suen, S.F. Hung, Q. Quan, N. Zhang, Y.J. Xu, H.M. Chen, Electrocatalysis for the oxygen evolution reaction: recent development and future perspectives, Chem Soc Rev, 46 (2017) 337-365.
[6] M. Tahir, L. Pan, F. Idrees, X. Zhang, L. Wang, J.-J. Zou, Z.L. Wang, Electrocatalytic oxygen evolution reaction for energy conversion and storage: A comprehensive review, Nano Energy, 37 (2017) 136-157.
[7] Z.W. Seh, J. Kibsgaard, C.F. Dickens, I. Chorkendorff, J.K. Norskov, T.F. Jaramillo, Combining theory and experiment in electrocatalysis: Insights into materials design, Science, 355 (2017) eaad4998.
[8] C. Chen, Y. Kang, Z. Huo, Z. Zhu, W. Huang, H.L. Xin, J.D. Snyder, D. Li, J.A. Herron, M. Mavrikakis, M. Chi, K.L. More, Y. Li, N.M. Markovic, G.A. Somorjai, P. Yang, V.R. Stamenkovic, Highly crystalline multimetallic nanoframes with three-dimensional electrocatalytic surfaces, Science, 343 (2014) 1339-1343.
[9] H. Over, Surface chemistry of ruthenium dioxide in heterogeneous catalysis and electrocatalysis: from fundamental to applied research, Chem Rev, 112 (2012) 3356-3426.
[10] C.C. McCrory, S. Jung, J.C. Peters, T.F. Jaramillo, Benchmarking heterogeneous electrocatalysts for the oxygen evolution reaction, J Am Chem Soc, 135 (2013) 16977-16987.
[11] Y. Lee, J. Suntivich, K.J. May, E.E. Perry, Y. Shao-Horn, Synthesis and Activities of Rutile IrO2 and RuO2 Nanoparticles for Oxygen Evolution in Acid and Alkaline Solutions, J Phys Chem Lett, 3 (2012) 399-404.
[12] W. Sheng, H.A. Gasteiger, Y. Shao-Horn, Hydrogen Oxidation and Evolution Reaction Kinetics on Platinum: Acid vs Alkaline Electrolytes, J Electrochem Soc, 157 (2010) B1529.
[13] B. Xiong, L. Chen, J. Shi, Anion-Containing Noble-Metal-Free Bifunctional Electrocatalysts for Overall Water Splitting, ACS Catal, 8 (2018) 3688-3707.
[14] M.I. Jamesh, Recent progress on earth abundant hydrogen evolution reaction and oxygen evolution reaction bifunctional electrocatalyst for overall water splitting in alkaline media, J Power Sources, 333 (2016) 213-236.
[15] Y. Wang, B. Kong, D. Zhao, H. Wang, C. Selomulya, Strategies for developing transition metal phosphides as heterogeneous electrocatalysts for water splitting, Nano Today, 15 (2017) 26-55.
[16] F. Cheng, J. Chen, Metal–air batteries: from oxygen reduction electrochemistry to cathode catalysts, Chem Soc Rev, 41 (2012) 2172-2192.
[17] D.U. Lee, P. Xu, Z.P. Cano, A.G. Kashkooli, M.G. Park, Z. Chen, Recent progress and perspectives on bi-functional oxygen electrocatalysts for advanced rechargeable metal–air batteries, J Mater Chem A, 4 (2016) 7107-7134.
[18] Z.L. Wang, D. Xu, J.J. Xu, X.B. Zhang, Oxygen electrocatalysts in metal-air batteries: from aqueous to nonaqueous electrolytes, Chem Soc Rev, 43 (2014) 7746-7786.
[19] D.M. Alonso, S.G. Wettstein, J.A. Dumesic, Bimetallic catalysts for upgrading of biomass to fuels and chemicals, Chem Soc Rev, 41 (2012) 8075-8098.
[20] Y.J. Wang, N.N. Zhao, B.Z. Fang, H. Li, X.T.T. Bi, H.J. Wang, Carbon-Supported Pt-Based Alloy Electrocatalysts for the Oxygen Reduction Reaction in Polymer Electrolyte Membrane Fuel Cells: Particle Size, Shape, and Composition Manipulation and Their Impact to Activity, Chem Rev, 115 (2015) 3433-3467.
[21] C.H. Cui, S.H. Yu, Engineering Interface and Surface of Noble Metal Nanoparticle Nanotubes toward Enhanced Catalytic Activity for Fuel Cell Applications, Acc Chem Res, 46 (2013) 1427-1437.
[22] Z.W. Quan, Y.X. Wang, J.Y. Fang, High-Index Faceted Noble Metal Nanocrystals, Acc Chem Res, 46

(2013) 191-202.
[23] B.E. Hayden, Particle Size and Support Effects in Electrocatalysis, Acc Chem Res, 46 (2013) 1858-1866.
[24] D.K. Perivoliotis, N. Tagmatarchis, Recent advancements in metal-based hybrid electrocatalysts supported on graphene and related 2D materials for the oxygen reduction reaction, Carbon, 118 (2017) 493-510.
[25] N.S. Porter, H. Wu, Z.W. Quan, J.Y. Fang, Shape-Control and Electrocatalytic Activity-Enhancement of Pt-Based Bimetallic Nanocrystals, Acc Chem Res, 46 (2013) 1867-1877.
[26] J.Y. Chen, B. Lim, E.P. Lee, Y.N. Xia, Shape-controlled synthesis of platinum nanocrystals for catalytic and electrocatalytic applications, Nano Today, 4 (2009) 81-95.
[27] T. Asefa, Metal-Free and Noble Metal-Free Heteroatom-Doped Nanostructured Carbons as Prospective Sustainable Electrocatalysts, Acc Chem Res, 49 (2016) 1873-1883.
[28] Y.P. Zhu, C. Guo, Y. Zheng, S.Z. Qiao, Surface and Interface Engineering of Noble-Metal-Free Electrocatalysts for Efficient Energy Conversion Processes, Acc Chem Res, 50 (2017) 915-923.
[29] X. Zou, Y. Zhang, Noble metal-free hydrogen evolution catalysts for water splitting, Chem Soc Rev, 44 (2015) 5148-5180.
[30] T. Wang, H. Xie, M. Chen, A. D'Aloia, J. Cho, G. Wu, Q. Li, Precious metal-free approach to hydrogen electrocatalysis for energy conversion: From mechanism understanding to catalyst design, Nano Energy, 42 (2017) 69-89.
[31] Y. Peng, B. Lu, S. Chen, Carbon-supported single atom catalysts for electrochemical energy conversion and storage, Adv Mater, (2018) 1801995.
[32] G.H. Wang, J. Hilgert, F.H. Richter, F. Wang, H.J. Bongard, B. Spliethoff, C. Weidenthaler, F. Schuth, Platinum-cobalt bimetallic nanoparticles in hollow carbon nanospheres for hydrogenolysis of 5-hydroxymethylfurfural, Nat Mater, 13 (2014) 293-300.
[33] X. Pan, Z. Fan, W. Chen, Y. Ding, H. Luo, X. Bao, Enhanced ethanol production inside carbon-nanotube reactors containing catalytic particles, Nat Mater, 6 (2007) 507-511.
[34] Z. Wen, J. Liu, J. Li, Core/Shell Pt/C Nanoparticles Embedded in Mesoporous Carbon as a Methanol-Tolerant Cathode Catalyst in Direct Methanol Fuel Cells, Adv Mater, 20 (2008) 743-747.
[35] X. Cui, P. Ren, D. Deng, J. Deng, X. Bao, Single layer graphene encapsulating non-precious metals as high-performance electrocatalysts for water oxidation, Energy Environ Sci, 9 (2016) 123-129.
[36] H. Fei, Y. Yang, Z. Peng, G. Ruan, Q. Zhong, L. Li, E.L. Samuel, J.M. Tour, Cobalt nanoparticles embedded in nitrogen-doped carbon for the hydrogen evolution reaction, ACS Appl Mater Interfaces, 7 (2015) 8083-8087.
[37] Q. Mo, N. Chen, M. Deng, L. Yang, Q. Gao, Metallic Cobalt@Nitrogen-Doped Carbon Nanocomposites: Carbon-Shell Regulation toward Efficient Bi-Functional Electrocatalysis, ACS Appl Mater Interfaces, 9 (2017) 37721-37730.
[38] X. Dai, Z. Li, Y. Ma, M. Liu, K. Du, H. Su, H. Zhuo, L. Yu, H. Sun, X. Zhang, Metallic Cobalt Encapsulated in Bamboo-Like and Nitrogen-Rich Carbonitride Nanotubes for Hydrogen Evolution Reaction, ACS Appl Mater Interfaces, 8 (2016) 6439-6448.
[39] H. Zhang, Z. Ma, J. Duan, H. Liu, G. Liu, T. Wang, K. Chang, M. Li, L. Shi, X. Meng, K. Wu, J. Ye, Active Sites Implanted Carbon Cages in Core-Shell Architecture: Highly Active and Durable Electrocatalyst for Hydrogen Evolution Reaction, ACS Nano, 10 (2016) 684-694.
[40] X. Zou, X. Huang, A. Goswami, R. Silva, B.R. Sathe, E. Mikmekova, T. Asefa, Cobalt-embedded nitrogen-rich carbon nanotubes efficiently catalyze hydrogen evolution reaction at all pH values, Angew Chem Int Ed, 53 (2014) 4372-4376.
[41] F. Lyu, Q. Wang, H. Zhu, M. Du, L. Wang, X. Zhang, A host-guest approach to fabricate metallic cobalt nanoparticles embedded in silk-derived N-doped carbon fibers for efficient hydrogen evolution, Green Energy & Environment, 2 (2017) 151-159.
[42] D. Hou, W. Zhou, K. Zhou, Y. Zhou, J. Zhong, L. Yang, J. Lu, G. Li, S. Chen, Flexible and porous catalyst electrodes constructed by Co nanoparticles@nitrogen-doped graphene films for highly efficient hydrogen evolution, J Mater Chem A, 3 (2015) 15962-15968.
[43] Z. Zhang, S. Liu, X. Tian, J. Wang, P. Xu, F. Xiao, S. Wang, Facile synthesis of N-doped porous carbon encapsulated bimetallic PdCo as a highly active and durable electrocatalyst for oxygen reduction and ethanol oxidation, J Mater Chem A, 5 (2017) 10876-10884.
[44] J. Chen, G. Xia, P. Jiang, Y. Yang, R. Li, R. Shi, J. Su, Q. Chen, Active and Durable Hydrogen Evolution Reaction Catalyst Derived from Pd-Doped Metal-Organic Frameworks, ACS Appl Mater

Interfaces, 8 (2016) 13378-13383.
[45] J. Su, Y. Yang, G. Xia, J. Chen, P. Jiang, Q. Chen, Ruthenium-cobalt nanoalloys encapsulated in nitrogen-doped graphene as active electrocatalysts for producing hydrogen in alkaline media, Nat Commun, 8 (2017) 14969.
[46] P. Jiang, J. Chen, C. Wang, K. Yang, S. Gong, S. Liu, Z. Lin, M. Li, G. Xia, Y. Yang, J. Su, Q. Chen, Tuning the Activity of Carbon for Electrocatalytic Hydrogen Evolution via an Iridium-Cobalt Alloy Core Encapsulated in Nitrogen-Doped Carbon Cages, Adv Mater, 30 (2018) 1705324.
[47] Y. Zheng, Y. Jiao, L.H. Li, T. Xing, Y. Chen, M. Jaroniec, S.Z. Qiao, Toward design of synergistically active carbon-based catalysts for electrocatalytic hydrogen evolution, ACS Nano, 8 (2014) 5290-5296.
[48] J.K. Norskov, T. Bligaard, J. Rossmeisl, C.H. Christensen, Towards the computational design of solid catalysts, Nat Chem, 1 (2009) 37-46.
[49] L. Yu, X. Pan, X. Cao, P. Hu, X. Bao, Oxygen reduction reaction mechanism on nitrogen-doped graphene: A density functional theory study, J Catal, 282 (2011) 183-190.
[50] E. Skulason, G.S. Karlberg, J. Rossmeisl, T. Bligaard, J. Greeley, H. Jonsson, J.K. Norskov, Density functional theory calculations for the hydrogen evolution reaction in an electrochemical double layer on the Pt(111) electrode, Phys Chem Chem Phys, 9 (2007) 3241-3250.
[51] L. Zhang, J. Niu, L. Dai, Z. Xia, Effect of microstructure of nitrogen-doped graphene on oxygen reduction activity in fuel cells, Langmuir, 28 (2012) 7542-7550.
[52] J.K. Nørskov, J. Rossmeisl, A. Logadottir, L.R. Lindqvist, J.R. Kitchin, T. Bligaard, H. Jonsson, Origin of the overpotential for oxygen reduction at a fuel-cell cathode, J Phys Chem B, 108 (2004) 17886-17892.
[53] E. Skúlason, V. Tripkovic, M.E. Björketun, S. Gudmundsdóttir, G. Karlberg, J. Rossmeisl, T. Bligaard, H. Jónsson, J.K. Nørskov, Modeling the electrochemical hydrogen oxidation and evolution reactions on the basis of density functional theory calculations, J Phys Chem C, 114 (2010) 18182-18197.
[54] Y. Li, H. Wang, L. Xie, Y. Liang, G. Hong, H. Dai, MoS2 nanoparticles grown on graphene: an advanced catalyst for the hydrogen evolution reaction, J Am Chem Soc, 133 (2011) 7296-7299.
[55] W. Zhou, J. Zhou, Y. Zhou, J. Lu, K. Zhou, L. Yang, Z. Tang, L. Li, S. Chen, N-Doped Carbon-Wrapped Cobalt Nanoparticles on N-Doped Graphene Nanosheets for High-Efficiency Hydrogen Production, Chem Mater, 27 (2015) 2026-2032.
[56] R. Parsons, The rate of electrolytic hydrogen evolution and the heat of adsorption of hydrogen, Trans Faraday Soc, 54 (1958) 1053-1063.
[57] J.K. Nørskov, T. Bligaard, A. Logadottir, J.R. Kitchin, J.G. Chen, S. Pandelov, U. Stimming, Trends in the Exchange Current for Hydrogen Evolution, J Electrochem Soc, 152 (2005) J23.
[58] J. Greeley, T.F. Jaramillo, J. Bonde, I.B. Chorkendorff, J.K. Norskov, Computational high-throughput screening of electrocatalytic materials for hydrogen evolution, Nat Mater, 5 (2006) 909-913.
[59] Y. Zheng, Y. Jiao, Y. Zhu, L.H. Li, Y. Han, Y. Chen, A. Du, M. Jaroniec, S.Z. Qiao, Hydrogen evolution by a metal-free electrocatalyst, Nat Commun, 5 (2014) 3783.
[60] J. Deng, P. Ren, D. Deng, X. Bao, Enhanced electron penetration through an ultrathin graphene layer for highly efficient catalysis of the hydrogen evolution reaction, Angew Chem Int Ed, 54 (2015) 2100-2104.
[61] W. Pei, S. Zhou, Y. Bai, J. Zhao, N-doped graphitic carbon materials hybridized with transition metals (compounds) for hydrogen evolution reaction: Understanding the synergistic effect from atomistic level, Carbon, 133 (2018) 260-266.
[62] B. Hammer, J.K. Norskov, Why gold is the noblest of all the metals, Nature, 376 (1995) 238.
[63] J. Rossmeisl, Z.W. Qu, H. Zhu, G.J. Kroes, J.K. Nørskov, Electrolysis of water on oxide surfaces, J Electroanal Chem, 607 (2007) 83-89.
[64] H. Dau, C. Limberg, T. Reier, M. Risch, S. Roggan, P. Strasser, The Mechanism of Water Oxidation: From Electrolysis via Homogeneous to Biological Catalysis, ChemCatChem, 2 (2010) 724-761.
[65] I.C. Man, H.-Y. Su, F. Calle-Vallejo, H.A. Hansen, J.I. Martínez, N.G. Inoglu, J. Kitchin, T.F. Jaramillo, J.K. Nørskov, J. Rossmeisl, Universality in Oxygen Evolution Electrocatalysis on Oxide Surfaces, ChemCatChem, 3 (2011) 1159-1165.
[66] R.V. Mom, J. Cheng, M.T.M. Koper, M. Sprik, Modeling the Oxygen Evolution Reaction on Metal Oxides: The Infuence of Unrestricted DFT Calculations, J Phys Chem C, 118 (2014) 4095-4102.
[67] P. Liao, J.A. Keith, E.A. Carter, Water oxidation on pure and doped hematite (0001) surfaces: prediction of Co and Ni as effective dopants for electrocatalysis, J Am Chem Soc, 134 (2012) 13296-13309.
[68] I.E. Stephens, A.S. Bondarenko, U. Grønbjerg, J. Rossmeisl, I. Chorkendorff, Understanding the

electrocatalysis of oxygen reduction on platinum and its alloys, Energy Environ Sci, 5 (2012) 6744-6762.
[69] F. Calle-Vallejo, M.T.M. Koper, First-principles computational electrochemistry: Achievements and challenges, Electrochim Acta, 84 (2012) 3-11.
[70] Y. Jiao, Y. Zheng, M. Jaroniec, S.Z. Qiao, Origin of the electrocatalytic oxygen reduction activity of graphene-based catalysts: a roadmap to achieve the best performance, J Am Chem Soc, 136 (2014) 4394-4403.
[71] B. Lu, T.J. Smart, D. Qin, J.E. Lu, N. Wang, L. Chen, Y. Peng, Y. Ping, S. Chen, Nitrogen and Iron-Codoped Carbon Hollow Nanotubules as High-Performance Catalysts toward Oxygen Reduction Reaction: A Combined Experimental and Theoretical Study, Chem Mater, 29 (2017) 5617-5628.
[72] F. Calle-Vallejo, J.I. Martinez, J. Rossmeisl, Density functional studies of functionalized graphitic materials with late transition metals for Oxygen Reduction Reactions, Phys Chem Chem Phys, 13 (2011) 15639-15643.
[73] I.C. Man, H.Y. Su, F. Calle-Vallejo, H.A. Hansen, J.I. Martínez, N.G. Inoglu, J. Kitchin, T.F. Jaramillo, J.K. Nørskov, J. Rossmeisl, Universality in oxygen evolution electrocatalysis on oxide surfaces. , ChemCatChem, 3 (2011) 1156-1165.
[74] S. Trasatti, Work function, electronegativity, and electrochemical behaviour of metals: III. Electrolytic hydrogen evolution in acid solutions, J Electroanal Chem Interfacial Electrochem, 39 (1972) 163-184.
[75] N.D. Lang, W. Kohn, Theory of Metal Surfaces: Work Function, Phys Rev B, 3 (1971) 1215-1223.
[76] F. Tao, M.E. Grass, Y. Zhang, D.R. Butcher, J.R. Renzas, Z. Liu, J.Y. Chung, B. Mun, M. Salmeron, G.A. Somorjai, Reaction-driven restructuring of Rh-Pd and Pt-Pd core-shell nanoparticles." Science, Science, 322 (2008) 932-934.
[77] Y. Xu, S. Yin, C. Li, K. Deng, H. Xue, X. Li, H. Wang, L. Wang, Low-ruthenium-content NiRu nanoalloys encapsulated in nitrogen-doped carbon as highly efficient and pH-universal electrocatalysts for the hydrogen evolution reaction, J Mater Chem A, 6 (2018) 1376-1381.
[78] Y. Xu, Y. Li, S. Yin, H. Yu, H. Xue, X. Li, H. Wang, L. Wang, Ultrathin nitrogen-doped graphitized carbon shell encapsulating CoRu bimetallic nanoparticles for enhanced electrocatalytic hydrogen evolution, Nanotechnology, 29 (2018) 225403.
[79] V. Di Noto, E. Negro, S. Polizzi, F. Agresti, G.A. Giffin, Synthesis-structure-morphology interplay of bimetallic "core-shell" carbon nitride nano-electrocatalysts, ChemSusChem, 5 (2012) 2451-2459.
[80] N. Du, C. Wang, R. Long, Y. Xiong, N-doped carbon-stabilized PtCo nanoparticles derived from Pt@ZIF-67: Highly active and durable catalysts for oxygen reduction reaction, Nano Res, 10 (2017) 3228-3237.
[81] Q. Jin, B. Ren, D. Li, H. Cui, C. Wang, Plasma-Assisted Synthesis of Self-Supporting Porous CoNPs@C Nanosheet as Efficient and Stable Bifunctional Electrocatalysts for Overall Water Splitting, ACS Appl Mater Interfaces, 9 (2017) 31913-31921.
[82] G. Zhang, P. Wang, W.T. Lu, C.Y. Wang, Y.K. Li, C. Ding, J. Gu, X.S. Zheng, F.F. Cao, Co Nanoparticles/Co, N, S Tri-doped Graphene Templated from In-Situ-Formed Co, S Co-doped g-C3N4 as an Active Bifunctional Electrocatalyst for Overall Water Splitting, ACS Appl Mater Interfaces, 9 (2017) 28566-28576.
[83] Z. Wang, S. Xiao, Z. Zhu, X. Long, X. Zheng, X. Lu, S. Yang, Cobalt-embedded nitrogen doped carbon nanotubes: a bifunctional catalyst for oxygen electrode reactions in a wide pH range, ACS Appl Mater Interfaces, 7 (2015) 4048-4055.
[84] H. Shao, X. Zhang, H. Huang, K. Zhang, M. Wang, C. Zhang, Y. Yang, M. Wen, W. Zheng, Magnetron Sputtering Deposition Cu@Onion-like N-C as High-Performance Electrocatalysts for Oxygen Reduction Reaction, ACS Appl Mater Interfaces, 9 (2017) 41945-41954.
[85] L. Ai, T. Tian, J. Jiang, Ultrathin Graphene Layers Encapsulating Nickel Nanoparticles Derived Metal–Organic Frameworks for Highly Efficient Electrocatalytic Hydrogen and Oxygen Evolution Reactions, ACS Sustain Chem Eng, 5 (2017) 4771-4777.
[86] Y. Hou, Z. Wen, S. Cui, S. Ci, S. Mao, J. Chen, An Advanced Nitrogen-Doped Graphene/Cobalt-Embedded Porous Carbon Polyhedron Hybrid for Efficient Catalysis of Oxygen Reduction and Water Splitting, Adv Funct Mater, 25 (2015) 872-882.
[87] M. Zeng, Y. Liu, F. Zhao, K. Nie, N. Han, X. Wang, W. Huang, X. Song, J. Zhong, Y. Li, Metallic Cobalt Nanoparticles Encapsulated in Nitrogen-Enriched Graphene Shells: Its Bifunctional Electrocatalysis and Application in Zinc-Air Batteries, Adv Funct Mater, 26 (2016) 4397-4404.
[88] Y.Z. Chen, C. Wang, Z.Y. Wu, Y. Xiong, Q. Xu, S.H. Yu, H.L. Jiang, From Bimetallic Metal-Organic Framework to Porous Carbon: High Surface Area and Multicomponent Active Dopants for Excellent

Electrocatalysis, Adv Mater, 27 (2015) 5010-5016.
[89] D. Deng, L. Yu, X. Chen, G. Wang, L. Jin, X. Pan, J. Deng, G. Sun, X. Bao, Iron encapsulated within pod-like carbon nanotubes for oxygen reduction reaction, Angew Chem Int Ed, 52 (2013) 371-375.
[90] S. Zhang, X. Xiao, T. Lv, X. Lv, B. Liu, W. Wei, J. Liu, Cobalt encapsulated N-doped defect-rich carbon nanotube as pH universal hydrogen evolution electrocatalyst, Appl Surf Sci, 446 (2018) 10-17.
[91] S. Zhang, Y. Zhang, W. Jiang, X. Liu, S. Xu, R. Huo, F. Zhang, J.-S. Hu, Co@N-CNTs derived from triple-role CoAl-layered double hydroxide as an efficient catalyst for oxygen reduction reaction, Carbon, 107 (2016) 162-170.
[92] Z.-Y. Chen, Y.-N. Yu, S.-J. Bao, M.-Q. Wang, Y.-N. Li, M.-w. Xu, Ascorbic acid-tailored synthesis of carbon-wrapped nanocobalt encapsulated in graphene aerogel as electrocatalysts for highly effective oxygen-reduction reaction, J Solid State Electr, 21 (2017) 3641-3648.
[93] F. Yang, P. Zhao, X. Hua, W. Luo, G. Cheng, W. Xing, S. Chen, A cobalt-based hybrid electrocatalyst derived from a carbon nanotube inserted metal–organic framework for efficient water-splitting, J Mater Chem A, 4 (2016) 16057-16063.
[94] Y. Zhao, J. Zhang, K. Li, Z. Ao, C. Wang, H. Liu, K. Sun, G. Wang, Electrospun cobalt embedded porous nitrogen doped carbon nanofibers as an efficient catalyst for water splitting, J Mater Chem A, 4 (2016) 12818-12824.
[95] S.H. Noh, M.H. Seo, X. Ye, Y. Makinose, T. Okajima, N. Matsushita, B. Han, T. Ohsaka, Design of an active and durable catalyst for oxygen reduction reactions using encapsulated Cu with N-doped carbon shells (Cu@N-C) activated by CO2 treatment, J Mater Chem A, 3 (2015) 22031-22034.
[96] T. Wang, Q. Zhou, X. Wang, J. Zheng, X. Li, MOF-derived surface modified Ni nanoparticles as an efficient catalyst for the hydrogen evolution reaction, J Mater Chem A, 3 (2015) 16435-16439.
[97] Y. Liu, H. Jiang, Y. Zhu, X. Yang, C. Li, Transition metals (Fe, Co, and Ni) encapsulated in nitrogen-doped carbon nanotubes as bi-functional catalysts for oxygen electrode reactions, J Mater Chem A, 4 (2016) 1694-1701.
[98] G. Zhang, W. Lu, F. Cao, Z. Xiao, X. Zheng, N-doped graphene coupled with Co nanoparticles as an efficient electrocatalyst for oxygen reduction in alkaline media, J Power Sources, 302 (2016) 114-125.
[99] W. Yang, L. Chen, X. Liu, J. Jia, S. Guo, A new method for developing defect-rich graphene nanoribbons/onion-like carbon@Co nanoparticles hybrid materials as an excellent catalyst for oxygen reactions, Nanoscale, 9 (2017) 1738-1744.
[100] Y. Tu, H. Li, D. Deng, J. Xiao, X. Cui, D. Ding, M. Chen, X. Bao, Low charge overpotential of lithium-oxygen batteries with metallic Co encapsulated in single-layer graphene shell as the catalyst, Nano Energy, 30 (2016) 877-884.
[101] Z. Wang, Y. Lu, Y. Yan, T.Y.P. Larissa, X. Zhang, D. Wuu, H. Zhang, Y. Yang, X. Wang, Core-shell carbon materials derived from metal-organic frameworks as an efficient oxygen bifunctional electrocatalyst, Nano Energy, 30 (2016) 368-378.
[102] Y. Su, Y. Zhu, H. Jiang, J. Shen, X. Yang, W. Zou, J. Chen, C. Li, Cobalt nanoparticles embedded in N-doped carbon as an efficient bifunctional electrocatalyst for oxygen reduction and evolution reactions, Nanoscale, 6 (2014) 15080-15089.
[103] F. Lei, W. Liu, Y. Sun, J. Xu, K. Liu, L. Liang, T. Yao, B. Pan, S. Wei, Y. Xie, Metallic tin quantum sheets confined in graphene toward high-efficiency carbon dioxide electroreduction, Nat Commun, 7 (2016) 12697.
[104] J.-S. Li, B. Du, Z.-H. Lu, Q.-T. Meng, J.-Q. Sha, In situ-generated Co@nitrogen-doped carbon nanotubes derived from MOFs for efficient hydrogen evolution under both alkaline and acidic conditions, New J Chem, 41 (2017) 10966-10971.
[105] W. Zhou, T. Xiong, C. Shi, J. Zhou, K. Zhou, N. Zhu, L. Li, Z. Tang, S. Chen, Bioreduction of Precious Metals by Microorganism: Efficient Gold@N-Doped Carbon Electrocatalysts for the Hydrogen Evolution Reaction, Angew Chem Int Ed, 55 (2016) 8416-8420.
[106] J. Lu, W. Zhou, L. Wang, J. Jia, Y. Ke, L. Yang, K. Zhou, X. Liu, Z. Tang, L. Li, S. Chen, Core–Shell Nanocomposites Based on Gold Nanoparticle@Zinc–Iron-Embedded Porous Carbons Derived from Metal–Organic Frameworks as Efficient Dual Catalysts for Oxygen Reduction and Hydrogen Evolution Reactions, ACS Catal, 6 (2016) 1045-1053.
[107] Y. Yang, Z. Lin, S. Gao, J. Su, Z. Lun, G. Xia, J. Chen, R. Zhang, Q. Chen, Tuning Electronic Structures of Nonprecious Ternary Alloys Encapsulated in Graphene Layers for Optimizing Overall Water Splitting Activity, ACS Catal, 7 (2016) 469-479.
[108] H.-X. Zhong, J. Wang, Q. Zhang, F. Meng, D. Bao, T. Liu, X.-Y. Yang, Z.-W. Chang, J.-M. Yan, X.-B.

Zhang, In Situ Coupling FeM (M = Ni, Co) with Nitrogen-Doped Porous Carbon toward Highly Efficient Trifunctional Electrocatalyst for Overall Water Splitting and Rechargeable Zn-Air Battery, Adv Sustainable Syst, 1 (2017) 1700020.
[109] Y. Shen, Y. Zhou, D. Wang, X. Wu, J. Li, J. Xi, Nickel-Copper Alloy Encapsulated in Graphitic Carbon Shells as Electrocatalysts for Hydrogen Evolution Reaction, Adv Energy Mater, 8 (2018) 1701759.
[110] H. Guo, N. Youliwasi, L. Zhao, Y. Chai, C. Liu, Carbon-encapsulated nickel-cobalt alloys nanoparticles fabricated via new post-treatment strategy for hydrogen evolution in alkaline media, Appl Surf Sci, 435 (2018) 237-246.
[111] A. Sivanantham, S. Shanmugam, Graphitic Carbon-NiCo Nanostructures as Efficient Non-Precious-Metal Electrocatalysts for the Oxygen Reduction Reaction, ChemElectroChem, (2018) https://doi.org/10.1002/celc.201800081.
[112] L. Zeng, X. Cui, L. Chen, T. Ye, W. Huang, R. Ma, X. Zhang, J. Shi, Non-noble bimetallic alloy encased in nitrogen-doped nanotubes as a highly active and durable electrocatalyst for oxygen reduction reaction, Carbon, 114 (2017) 347-355.
[113] X. Zhong, Y. Qin, X. Chen, W. Xu, G. Zhuang, X. Li, J. Wang, PtPd alloy embedded in nitrogen-rich graphene nanopores: High-performance bifunctional electrocatalysts for hydrogen evolution and oxygen reduction, Carbon, 114 (2017) 740-748.
[114] J. Long, R. Li, X. Gou, Well-organized Co-Ni@NC material derived from hetero-dinuclear MOFs as efficient electrocatalysts for oxygen reduction, Catal Commun, 95 (2017) 31-35.
[115] S. Saha, A.K. Ganguli, FeCoNi Alloy as Noble Metal-Free Electrocatalyst for Oxygen Evolution Reaction (OER), ChemistrySelect, 2 (2017) 1630-1636.
[116] Y. Yang, Z. Lun, G. Xia, F. Zheng, M. He, Q. Chen, Non-precious alloy encapsulated in nitrogen-doped graphene layers derived from MOFs as an active and durable hydrogen evolution reaction catalyst, Energy Environ Sci, 8 (2015) 3563-3571.
[117] J. Yu, Y. Zhong, W. Zhou, Z. Shao, Facile synthesis of nitrogen-doped carbon nanotubes encapsulating nickel cobalt alloys 3D networks for oxygen evolution reaction in an alkaline solution, J Power Sources, 338 (2017) 26-33.
[118] G. Fu, Y. Chen, Z. Cui, Y. Li, W. Zhou, S. Xin, Y. Tang, J.B. Goodenough, Novel Hydrogel-Derived Bifunctional Oxygen Electrocatalyst for Rechargeable Air Cathodes, Nano Lett, 16 (2016) 6516-6522.
[119] B. Bayatsarmadi, Y. Zheng, V. Russo, L. Ge, C.S. Casari, S.Z. Qiao, Highly active nickel-cobalt/nanocarbon thin films as efficient water splitting electrodes, Nanoscale, 8 (2016) 18507-18515.
[120] B. Du, Q.-T. Meng, J.-Q. Sha, J.-S. Li, Facile synthesis of FeCo alloys encapsulated in nitrogen-doped graphite/carbon nanotube hybrids: efficient bi-functional electrocatalysts for oxygen and hydrogen evolution reactions, New Journal of Chemistry, 42 (2018) 3409-3414.
[121] S.H. Noh, M.H. Seo, J. Kang, T. Okajima, B. Han, T. Ohsaka, Towards a comprehensive understanding of FeCo coated with N-doped carbon as a stable bi-functional catalyst in acidic media, NPG Asia Mater, 8 (2016) e312-e312.
[122] X. Duan, J. Xu, Z. Wei, J. Ma, S. Guo, S. Wang, H. Liu, S. Dou, Metal-Free Carbon Materials for CO2 Electrochemical Reduction, Adv Mater, 29 (2017).
[123] L. Dai, Y. Xue, L. Qu, H.J. Choi, J.B. Baek, Metal-free catalysts for oxygen reduction reaction, Chem Rev, 115 (2015) 4823-4892.
[124] J.P. Paraknowitsch, A. Thomas, Doping carbons beyond nitrogen: an overview of advanced heteroatom doped carbons with boron, sulphur and phosphorus for energy applications, Energy Environ Sci, 6 (2013) 2839.
[125] D.-W. Wang, D. Su, Heterogeneous nanocarbon materials for oxygen reduction reaction, Energy Environ Sci, 7 (2014) 576.
[126] L. Yang, W. Zhou, J. Jia, T. Xiong, K. Zhou, C. Feng, J. Zhou, Z. Tang, S. Chen, Nickel nanoparticles partially embedded into carbon fiber cloth via metal-mediated pitting process as flexible and efficient electrodes for hydrogen evolution reactions, Carbon, 122 (2017) 710-717.
[127] J. Deng, L. Yu, D. Deng, X. Chen, F. Yang, X. Bao, Highly active reduction of oxygen on a FeCo alloy catalyst encapsulated in pod-like carbon nanotubes with fewer walls, J Mater Chem A, 1 (2013) 14868.
[128] M. Tavakkoli, T. Kallio, O. Reynaud, A.G. Nasibulin, C. Johans, J. Sainio, H. Jiang, E.I. Kauppinen, K. Laasonen, Single-shell carbon-encapsulated iron nanoparticles: synthesis and high electrocatalytic activity for hydrogen evolution reaction, Angew Chem Int Ed, 54 (2015) 4535-4538.
[129] J. Yu, W. Zhou, T. Xiong, A. Wang, S. Chen, B. Chu, Enhanced electrocatalytic activity of Co@N-

doped carbon nanotubes by ultrasmall defect-rich TiO2 nanoparticles for hydrogen evolution reaction, Nano Res, 10 (2017) 2599-2609.
[130] H. Jin, J. Wang, D. Su, Z. Wei, Z. Pang, Y. Wang, In situ cobalt-cobalt oxide/N-doped carbon hybrids as superior bifunctional electrocatalysts for hydrogen and oxygen evolution, J Am Chem Soc, 137 (2015) 2688-2694.
[131] A. Aijaz, J. Masa, C. Rosler, W. Xia, P. Weide, A.J. Botz, R.A. Fischer, W. Schuhmann, M. Muhler, Co@Co3O4 Encapsulated in Carbon Nanotube-Grafted Nitrogen-Doped Carbon Polyhedra as an Advanced Bifunctional Oxygen Electrode, Angew Chem Int Ed, 55 (2016) 4087-4091.
[132] J. Hou, Y. Sun, Y. Wu, S. Cao, L. Sun, Promoting Active Sites in Core-Shell Nanowire Array as Mott-Schottky Electrocatalysts for Efficient and Stable Overall Water Splitting, Adv Funct Mater, 28 (2018) 1704447.
[133] H. Zhuang, Y. Xie, H. Tan, Y. Deng, Y. Li, G. Chen, CoFe x -CoFe 2 O 4 /N-doped carbon nanocomposite derived from in situ pyrolysis of a single source precursor as a superior bifunctional electrocatalyst for water splitting, Electrochim Acta, 262 (2018) 18-26.
[134] Y. Ma, X. Dai, M. Liu, J. Yong, H. Qiao, A. Jin, Z. Li, X. Huang, H. Wang, X. Zhang, Strongly Coupled FeNi Alloys/NiFe2O4@Carbonitride Layers-Assembled Microboxes for Enhanced Oxygen Evolution Reaction, ACS Appl Mater Interfaces, 8 (2016) 34396-34404.
[135] X. Yan, L. Tian, M. He, X. Chen, Three-Dimensional Crystalline/Amorphous Co/Co3O4 Core/Shell Nanosheets as Efficient Electrocatalysts for the Hydrogen Evolution Reaction, Nano Lett, 15 (2015) 6015-6021.
[136] X. Yan, L. Tian, X. Chen, Crystalline/amorphous Ni/NiO core/shell nanosheets as highly active electrocatalysts for hydrogen evolution reaction, J Power Sources, 300 (2015) 336-343.
[137] Z. Wen, S. Ci, F. Zhang, X. Feng, S. Cui, S. Mao, S. Luo, Z. He, J. Chen, Nitrogen-enriched core-shell structured Fe/Fe(3)C-C nanorods as advanced electrocatalysts for oxygen reduction reaction, Adv Mater, 24 (2012) 1399-1404.
[138] Y. Hou, T. Huang, Z. Wen, S. Mao, S. Cui, J. Chen, Metal−Organic Framework-Derived Nitrogen-Doped Core-Shell-Structured Porous Fe/Fe3
C@C Nanoboxes Supported on Graphene Sheets for Efficient Oxygen Reduction Reactions, Adv Energy Mater, 4 (2014) 1400337.
[139] Q. Wang, Y. Lei, Z. Chen, N. Wu, Y. Wang, B. Wang, Y. Wang, Fe/Fe3C@C nanoparticles encapsulated in N-doped graphene–CNTs framework as an efficient bifunctional oxygen electrocatalyst for robust rechargeable Zn–air batteries, J Mater Chem A, 6 (2018) 516-526.
[140] X. Chen, J. Xiao, J. Wang, D. Deng, Y. Hu, J. Zhou, L. Yu, T. Heine, X. Pan, X. Bao, Visualizing electronic interactions between iron and carbon by X-ray chemical imaging and spectroscopy, Chem Sci, 6 (2015) 3262-3267.
[141] R.A. Sidik, A.B. Anderson, Co9S8 as a catalyst for electroreduction of O2: quantum chemistry predictions, J Phys Chem. B, 110 (2006) 936-941.
[142] J. Yang, G. Zhu, Y. Liu, J. Xia, Z. Ji, X. Shen, S. Wu, Fe3O4-Decorated Co9S8Nanoparticles In Situ Grown on Reduced Graphene Oxide: A New and Efficient Electrocatalyst for Oxygen Evolution Reaction, Adv Funct Mater, 26 (2016) 4712-4721.
[143] X. Zhang, S. Liu, Y. Zang, R. Liu, G. Liu, G. Wang, Y. Zhang, H. Zhang, H. Zhao, Co/Co 9 S 8 @S,N-doped porous graphene sheets derived from S, N dual organic ligands assembled Co-MOFs as superior electrocatalysts for full water splitting in alkaline media, Nano Energy, 30 (2016) 93-102.
[144] R. Li, Y. Dai, B. Chen, J. Zou, B. Jiang, H. Fu, Nitrogen-doped Co/Co 9 S 8 /partly-graphitized carbon as durable catalysts for oxygen reduction in microbial fuel cells, J Mater Chem A, 307 (2016) 1-10.
[145] Y. Hao, Y. Xu, W. Liu, X. Sun, Co/CoP embedded in a hairy nitrogen-doped carbon polyhedron as an advanced tri-functional electrocatalyst, Mater Horiz, 5 (2018) 108-115.
[146] J. Tian, Q. Liu, A.M. Asiri, X. Sun, Self-supported nanoporous cobalt phosphide nanowire arrays: an efficient 3D hydrogen-evolving cathode over the wide range of pH 0-14, J Am Chem Soc, 136 (2014) 7587-7590.
[147] Q. Liu, J. Tian, W. Cui, P. Jiang, N. Cheng, A.M. Asiri, X. Sun, Carbon nanotubes decorated with CoP nanocrystals: a highly active non-noble-metal nanohybrid electrocatalyst for hydrogen evolution, Angew Chem Int Ed, 53 (2014) 6710-6714.
[148] E.J. Popczun, C.G. Read, C.W. Roske, N.S. Lewis, R.E. Schaak, Highly active electrocatalysis of the hydrogen evolution reaction by cobalt phosphide nanoparticles, Angew Chem Int Ed, 53 (2014) 5427-5430.

[149] Q. Jin, B. Ren, D. Li, H. Cui, C. Wang, In situ promoting water dissociation kinetic of Co based electrocatalyst for unprecedentedly enhanced hydrogen evolution reaction in alkaline media, Nano Energy, 49 (2018) 14-22.
[150] W. Xia, R. Zou, L. An, D. Xia, S. Guo, A metal–organic framework route to in situ encapsulation of Co@Co3O4@C core@bishell nanoparticles into a highly ordered porous carbon matrix for oxygen reduction, Energy Environ Sci, 8 (2015) 568-576.
[151] Z. Li, M. Shao, L. Zhou, R. Zhang, C. Zhang, M. Wei, D.G. Evans, X. Duan, Directed Growth of Metal-Organic Frameworks and Their Derived Carbon-Based Network for Efficient Electrocatalytic Oxygen Reduction, Adv Mater, 28 (2016) 2337-2344.
[152] Y.V. Kaneti, J. Tang, R.R. Salunkhe, X. Jiang, A. Yu, K.C. Wu, Y. Yamauchi, Nanoarchitectured Design of Porous Materials and Nanocomposites from Metal-Organic Frameworks, Adv Mater, 29 (2017) 1604898.
[153] J. Liu, D. Zhu, C. Guo, A. Vasileff, S.-Z. Qiao, Design Strategies toward Advanced MOF-Derived Electrocatalysts for Energy-Conversion Reactions, Adv Energy Mater, 7 (2017) 1700518.
[154] A.A. Gewirth, J.A. Varnell, A.M. DiAscro, Nonprecious Metal Catalysts for Oxygen Reduction in Heterogeneous Aqueous Systems, Chem Rev, 118 (2018) 2313-2339.
[155] M. Zhou, H.L. Wang, S. Guo, Towards high-efficiency nanoelectrocatalysts for oxygen reduction through engineering advanced carbon nanomaterials, Chem Soc Rev, 45 (2016) 1273-1307.
[156] B.Y. Guan, X.Y. Yu, H.B. Wu, X.W.D. Lou, Complex Nanostructures from Materials based on Metal-Organic Frameworks for Electrochemical Energy Storage and Conversion, Adv Mater, 29 (2017) 1703614.
[157] H.B. Yang, J. Miao, S.F. Hung, J. Chen, H.B. Tao, X. Wang, L. Zhang, R. Chen, J. Gao, H.M. Chen, L. Dai, Identification of catalytic sites for oxygen reduction and oxygen evolution in N-doped graphene materials: Development of highly efficient metal-free bifunctional electrocatalyst, Sci Adv, 2 (2016) e1501122.
[158] G. Fu, Z. Cui, Y. Chen, Y. Li, Y. Tang, J.B. Goodenough, Ni3Fe-N Doped Carbon Sheets as a Bifunctional Electrocatalyst for Air Cathodes, Adv Energy Mater, 7 (2017) 1601172.
[159] X. Han, X. Wu, C. Zhong, Y. Deng, N. Zhao, W. Hu, NiCo 2 S 4 nanocrystals anchored on nitrogen-doped carbon nanotubes as a highly efficient bifunctional electrocatalyst for rechargeable zinc-air batteries, Nano Energy, 31 (2017) 541-550.
[160] J. Zhang, Z. Zhao, Z. Xia, L. Dai, A metal-free bifunctional electrocatalyst for oxygen reduction and oxygen evolution reactions, Nat Nanotechnol, 10 (2015) 444-452.

Yi Peng received his B.S. degree in Chemistry in 2014 from Beihang University, Beijing, China, and then went to the University of California at Santa Cruz (UCSC) to pursue his Ph.D. degree in Chemistry under the supervisor of Prof. Shaowei Chen. In 2017, he received the John and Grace Wang Award in Physical Chemistry and a STEM Chateaubriand Fellowship. He was also awarded the 2018 Joseph W. Richards Summer Fellowship from the Electrochemical Society, and the Chancellor's Dissertation Year Fellowship. His research interests include metal/semiconductor nanoparticle surface functionalization, nanoparticle charge-transfer dynamics, and single atom catalysts for electrochemical energy conversion and storage.

Shaowei Chen received his B.S. degree in Chemistry from USTC in 1991, and his M.S. and Ph.D. degrees from Cornell University in 1993 and 1996, respectively. Following a postdoctoral appointment in the University of North Carolina at Chapel Hill, he started his independent career in Southern Illinois University in 1998. In 2004, he moved to UCSC. He is currently a Professor of Chemistry and the Faculty Director of the UCSC COSMOS program. His research interests are primarily focused on high-performance catalysts for electrochemical energy conversion and storage, impacts of metal–ligand interfacial bonding interactions on nanoparticle charge-transfer dynamics, Janus nanoparticles by interfacial engineering, and antimicrobial activity of functional nanomaterials.